Contrib Mineral Petrol (2015) 170:22
DOI 10.1007/s00410-015-1181-0

ORIGINAL PAPER

# A trachyte–syenite core within a basaltic nest: filtering of primitive injections by a multi-stage magma plumbing system (Oki-Dōzen, south-west Japan)

**Marco Brenna[1,3] · Setsuya Nakada[1] · Daisuke Miura[2] · Kiyoshi Toshida[2] · Hisatoshi Ito[2] · Natsumi Hokanishi[1] · Shun'ichi Nakai[1]**

Received: 25 April 2015 / Accepted: 31 July 2015


**Abstract** Oki-Dōzen (Japan) is a Late Miocene (7–5 Ma) intraplate alkalic volcano composed of a central trachytic pyroclastic complex surrounded by a ring-shaped succession of basaltic to trachybasaltic lavas and pyroclastic rocks and dispersed trachytic bodies. The central trachytic complex is in contact with a syenite that was intruded into the basement early Miocene volcano-sedimentary succession. In the centre of the system there are no alkalic basaltic rocks that are correlative of the outer flank ring. We present whole-rock major and trace element chemistry, Sr–Nd–Pb isotopic compositions and petrological data from the central trachytic volcanic complex and the intrusive syenite body, as well as from the outer ring basaltic succession. We also present and discuss a new set of zircon U/Pb ages collected from the central trachyte and syenite bodies. All the eruptive products of Oki-Dōzen, as well as the syenite, plot on a single liquid line of descent initiated from a mantle-derived alkalic basaltic parent. A younger (2.8 Ma) basaltic eruption (Uzuka basalt) has isotopic compositions that distinguish it from the rest of the system. Geochemical modelling indicates that magmatic differentiation through crystal fractionation and minor crustal assimilation occurred in crustal and shallow sub-volcanic magma reservoirs. In the central part of the system, a number of vertically spaced reservoirs acted as a filter, capturing basaltic dykes and hindering their ascent. In the outer region, dykes either reached the surface unhindered and erupted to form the basaltic/trachybasaltic succession or stalled at crustal levels and differentiated to trachyte before forming dispersed domes/flows. The central plumbing system "filter" resulted in a nest-shaped volcano, with a trachytic core surrounded by basaltic products, and stopped direct injection of basaltic magmas into the shallow syenitic magma reservoir, likely preventing its destabilization and explosive eruption.

**Keywords** Oki-Dōzen · Intraplate alkalic volcanism · Whole-rock chemistry · Trachyte · Isotope composition · Multi-stage plumbing system · Thermobarometry

Communicated by Othmar Müntener.

**Electronic supplementary material** The online version of this article (doi:10.1007/s00410-015-1181-0) contains supplementary material, which is available to authorized users.

✉ Marco Brenna
m.brenna@auckland.ac.nz

[1] Earthquake Research Institute, University of Tokyo, 1-1-1 Yayoi, Bunkyo-ku, Tokyo 113-0032, Japan

[2] Geosphere Sciences, Civil Engineering Research Laboratory, Central Research Institute of Electric Power Industry, 1646 Abiko, Abiko 270-1194, Japan

[3] Present Address: School of Environment, The University of Auckland, Private Bag 92019, Auckland 1142, New Zealand

## Introduction

Alkalic intraplate volcanism is a widespread phenomenon on the Earth. It can range from relatively small "monogenetic" volcanic fields composed of a few dispersed small-volume vents of mainly alkalic basaltic compositions, such as the Auckland Volcanic Field in New Zealand (McGee et al. 2013), to large volcanic edifices consisting of evolved lavas ranging from phonolite to alkalic rhyolite, and capable of generating large caldera-forming eruptions, such as Changbaishan, China (Wei et al. 2007). There exists a plethora of intermediate examples on a scale between these very different types of intraplate volcanoes. Some

Published online: 08 August 2015

volcanic fields erupted dispersed trachytic/phonolitic lavas intercalated with basaltic flows without forming a central large volcanic edifice, such as the Meidob Volcanic Field, Sudan (Franz et al. 1997), the Eifel Volcanic Field, Germany (Wörner and Schmincke 1984), or the early magmatic phase of the Jeju Island Volcanic Field, Republic of Korea (Koh et al. 2013). In the latter, the system subsequently evolved and formed a central edifice constructed of series of basaltic to trachytic flows and domes without large explosive eruptions (Brenna et al. 2012). These diverse volcanic landforms and behaviours are due to different levels of complexity of the feeding magmatic systems.

The morphological surface expression of the magmatic system depends on several internal and external competing factors. Regional and local tectonic stresses can influence the plumbing system and result in variably dispersed volcanic landforms (Nakamura 1977; Takada 1994; Le Corvec et al. 2013). The crustal structure, coupled with magmatic viscosity and buoyancy, may facilitate or hinder the stalling of magma bodies and hence the generation of magma storage regions that result in progressive chemical evolution (Hansteen et al. 1998; Valentine and Krogh 2006; Diez et al. 2009). The site of magmatic differentiation and the rate of magma ascent and volatile exsolution may ultimately control the eruption style (Eichelberger et al. 1986; Andújar and Scaillet 2012; Brenna et al. 2014), although interaction with groundwater at shallow levels may increase the degree of explosivity (Zimanowski et al. 1997). In the case of caldera-forming eruptions, a large enough volume of magma is accumulated and erupted before catastrophic collapse of the magma reservoir's roof (Roche and Druitt 2001; Bachmann et al. 2002, 2012; Jellinek and DePaolo 2003) in a process that can result in stress changes and lead to the migration of magma chambers and eruption sites (Marti and Gudmundsson 2000). Many processes are at play in controlling volcanic behaviour, and they are often recorded in the crystals contained within the magmas feeding the volcano. Additionally, explosive eruptions at intraplate alkalic volcanoes often carry (syenitic) xenoliths/autoliths of intrusive rocks that are representative of deeper portions of the plumbing system (Borley et al. 1971; Price et al. 2003; Brenna et al. 2014). Magmatic and foreign crystals can be interrogated to quantify the intensive parameters of magmatic evolution (e.g. pressure and temperature). In particular, recent predictive models specifically calibrated for alkalic systems enable unprecedented insights into the conditions of magmatic evolution at intraplate volcanoes (Ridolfi and Renzulli 2012; Masotta et al. 2013; Mollo et al. 2015).

Here we present an investigation of the Oki-Dōzen (Japan) volcano with the aim of constraining the properties of the plumbing system. Oki-Dōzen was active c. 7–5 Ma, after the Sea of Japan formed 21–14 Ma (Otofuji et al. 1985) and is built on continental crust (Tamaki et al. 1992). Geological contacts exposed at Oki-Dōzen make it ideal for such a study. In particular, the core of Oki-Dōzen consists of a large trachytic body abutting a syenitic intrusion as well as older uplifted basement volcano-sedimentary rocks, thus representing an opportunity to study in situ an exposed magmatic reservoir associated with its consanguineous eruption products (Morris et al. 1997). We discuss new chemical, petrological and isotopic data, as well as a new set of chronological constraints for a suite of samples collected from around the island, with emphasis on rocks from the central complex. With the aid of the new predictive models, we quantify temperature and depth of magmatic evolution to reveal that a laterally and vertically complex plumbing system resulted in a nested silicic core surrounded by a ring dominated by more primitive lavas.

## Geological background

Oki-Dōzen has been the subject of numerous geological studies. It is situated in the southern part of the Sea of Japan, approximately 50 km to the north of the San'in coast, Shimane Prefecture, and approximately 15 km to the south-west of Oki-Dōgo Island. Oki-Dōzen consists of three main islands: Nishinoshima, Nakanoshima and Chiburijima. These are arranged so as to embrace a harbour, from which Takuhiyama (Mount Takuhi, part of Nishinoshima; Fig. 1) rises out of the centre. The Island is partially included in the Daisen-Oki National Park and has been awarded UNESCO Global Geopark status due to the number of excellent exposures of volcanic deposits.

Tiba (1986) proposed that the Oki-Dōzen volcano started with the formation of a basaltic to trachybasaltic ring-shaped edifice rather than a conical "shield" formed by dispersed eruptions (the "somma" phase). In Tiba's model, this was followed by a "non-explosive" subsidence caldera event that formed the central harbour (i.e. without accompanying voluminous pyroclastic flows) and subsequent central trachytic cone formation (Takuhiyama trachyte) as a post-caldera stage. Finally, further dispersed eruptions of basaltic to trachytic magma occurred on the outer flanks (Tiba 1986). Radiometric dating has led to the revision of the interpretation of the caldera formation and central cone trachyte eruption events (Tiba et al. 2000). According to K/Ar dating, the initial "somma" phase of dispersed volcanism occurred between 6.3 and 5.3 Ma with the eruption of the Takuhiyama trachyte at approximately 5.4 Ma (Morris et al. 1990, 1997; Wada et al. 1990; Tiba et al. 2000). This implies that a caldera formation occurred prior to 5.4 Ma. A final, anomalously young eruption (the Uzuka basalt) occurred on Nakanoshima c. 2.8 Ma and formed a scoria cone and lava flows (Kaneko and Tiba 1998; Fig. 1).

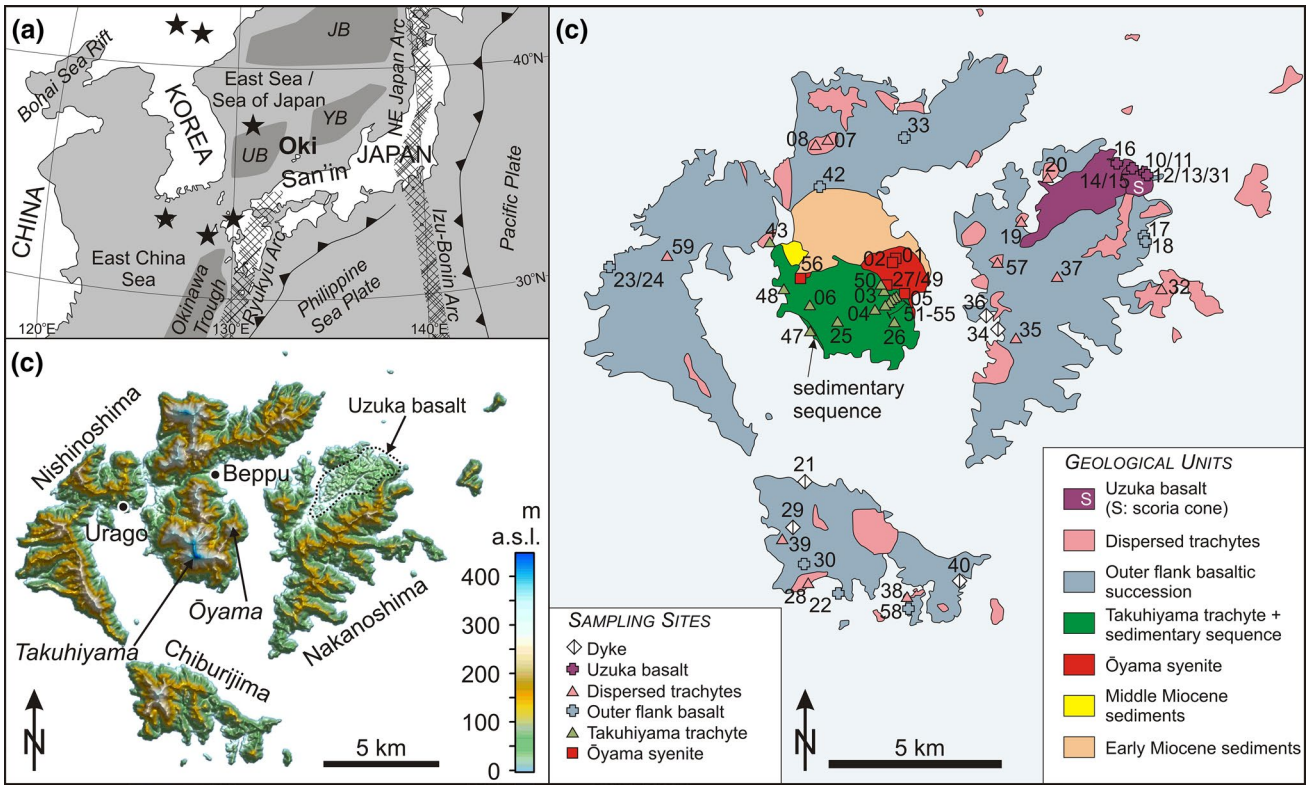


**Fig. 1** Regional and geological settings of Oki-Dōzen. **a** Location of Oki-Dōzen (Oki) with respect to regional tectonic features; *UB* Ulleung Basin, *YB* Yamato Basin, *JB* Japan Basin. The *stars* indicate major Quaternary intraplate volcanic activity. **b** Shaded digital elevation model of Oki-Dōzen showing the three main islands and the location of Takuhiyama and Ōyama. **c** Geological map of the main units at Oki-Dōzen based on Tiba et al. (2000). The *numbers* correlate to the presented DZ samples (DZ is omitted for clarity)

The Takuhiyama trachyte has sub-vertical contacts with a body of syenite (Ōyama syenite), which has yielded K/Ar ages of 7.4–6.3 Ma (Morris et al. 1997; Tiba et al. 2000) and is nowhere else exposed other than in the central portion of Oki-Dōzen. The Ōyama syenite intruded a sequence of early to middle Miocene volcanic (calc-alkaline) and sedimentary rocks (Tiba et al. 2000; Matsubara et al. 2014), which is uplifted and exposed along the ridge to the north of Takuhiyama (Naemura and Shimada 1984). The volcano-sedimentary sequence is folded to a broad NNW–SSE trending anticline and is intruded by NNW–SSE to N–S trending trachytic to rhyolitic dykes (Tiba et al. 2000). The syenite is considered the intrusive equivalent of the Takuhiyama trachyte (Morris et al. 1997) based on similar trace element and isotopic characteristics.

## Analytical procedure

Mineral chemistry was measured using a JXA8800R wavelength-dispersive electron-probe microanalyser (WDS-EPMA) with an accelerating voltage of 15 kV and a beam current of 12 nA at the Earthquake Research Institute (ERI) at the University of Tokyo. Beam diameter was set at 10 μm. Peak measuring times for major elements were 15–20 s. Mineral analyses are available as Electronic Appendix 1.

Whole-rock major and selected trace element compositions were determined by X-ray fluorescence (XRF) spectroscopy at the Earthquake Research Institute (ERI) at the University of Tokyo using a RIGAKU ZSX Primus II. $H_2O^-$ and LOI were measured by heating ~4 g of sample for 12 h at 105 °C and 4 h 1000 °C, respectively. Fused glass discs were prepared in Pt crucibles by mixing lithium tetraborate flux and 2 g of dry sample powder in a 5:1 mass ratio. Repeat analyses of standard JB-1a and JG-1a indicate precision and accuracy better than 5 % at the 95 % confidence level for most elements. Sampling locations are shown in Fig. 1, and representative analyses are reported in Table 1. The complete dataset is available as Electronics Appendix 2.

Sr, Nd and Pb isotopic ratios were determined by a multi-collector (MC)-ICP-MS (IsoProbe; GV Instruments) also at the Earthquake Research Institute (ERI) at the University of Tokyo. Ultrapure grade HF, $HClO_4$, $HNO_3$ and HCl (Kanto Chemical Co. Inc.) were used for analyses.

**Table 1** Major and trace element data for selected samples of Oki-Dōzen

| Sample | DZ01 | DZ02S | DZ03 | DZ05 | DZ06 | DZ15 | DZ20 | DZ23 | DZ24 |
|---|---|---|---|---|---|---|---|---|---|
| Geological unit | OS | OS | TT | OS | TT | UB | DT | OBS | OBS |
| $SiO_2$ | 65.30 | 63.33 | 69.31 | 65.67 | 64.79 | 48.02 | 62.99 | 45.25 | 50.22 |
| $TiO_2$ | 0.47 | 0.85 | 0.35 | 0.41 | 0.69 | 2.59 | 0.63 | 3.23 | 2.87 |
| $Al_2O_3$ | 17.39 | 16.94 | 15.44 | 17.70 | 17.73 | 15.97 | 17.56 | 13.13 | 17.79 |
| $FeO_{tot}$ | 3.45 | 4.34 | 2.91 | 3.17 | 3.28 | 9.35 | 4.55 | 12.72 | 9.58 |
| MnO | 0.18 | 0.20 | 0.08 | 0.19 | 0.08 | 0.15 | 0.18 | 0.17 | 0.17 |
| MgO | 0.31 | 0.71 | 0.24 | 0.30 | 0.53 | 9.37 | 0.95 | 11.66 | 4.37 |
| CaO | 0.49 | 1.78 | 0.29 | 0.70 | 1.22 | 9.42 | 1.97 | 9.81 | 7.65 |
| $Na_2O$ | 5.60 | 5.40 | 2.80 | 5.41 | 5.16 | 2.77 | 5.78 | 2.61 | 3.14 |
| $K_2O$ | 6.73 | 6.26 | 8.54 | 6.38 | 6.35 | 1.74 | 5.24 | 1.04 | 3.30 |
| $P_2O_5$ | 0.08 | 0.18 | 0.05 | 0.07 | 0.18 | 0.63 | 0.16 | 0.39 | 0.90 |
| TOT | 100.00 | 100.00 | 100.00 | 100.00 | 100.00 | 100.00 | 100.00 | 100.00 | 100.00 |
| $H_2O^-$ | 0.47 | 0.32 | 0.15 | 0.36 | 0.26 | 0.68 | 0.59 | 0.62 | 0.91 |
| LOI | 0.94 | 0.92 | 0.65 | 0.89 | 0.40 | 1.51 | 0.40 | 0.50 | 0.47 |
| Sc | 3 | 8 | 0 | 2 | 4 | 25 | 5 | 33 | 21 |
| V | 6 | 4 | 8 | 3 | 14 | 193 | 6 | 332 | 193 |
| Cr | 0 | bdl | bdl | bdl | bdl | 279 | bdl | 323 | 18 |
| Co | 1 | 2 | 2 | 1 | 3 | 44 | 2 | 69 | 31 |
| Ni | 6 | 3 | 6 | 5 | 5 | 240 | 3 | 170 | 22 |
| Cu | 6 | 4 | 8 | 6 | 5 | 51 | 6 | 27 | 21 |
| Zn | 86 | 93 | 120 | 105 | 104 | 77 | 109 | 91 | 97 |
| Ga | 22 | 20 | 24 | 24 | 24 | 18 | 24 | 18 | 21 |
| Rb | 161 | 128 | 306 | 153 | 118 | 68 | 134 | 13 | 71 |
| Y | 31 | 32 | 61 | 42 | 30 | 25 | 41 | 19 | 38 |
| Sr | 47 | 90 | 153 | 108 | 204 | 929 | 472 | 560 | 909 |
| Zr | 346 | 484 | 804 | 766 | 853 | 188 | 603 | 208 | 411 |
| Nb | 64 | 94 | 148 | 124 | 67 | 44 | 93 | 39 | 84 |
| Ba | 249 | 822 | 251 | 543 | 1191 | 764 | 1695 | 571 | 1231 |
| Pb | 13 | 13 | 23 | 22 | 16 | 5 | 14 | 5 | 10 |
| La | 99 | 57 | 174 | 196 | 78 | 38 | 99 | 42 | 107 |
| Ce | 188 | 151 | 310 | 365 | 208 | 99 | 280 | 106 | 237 |
| Th | 14 | 8 | 31 | 27 | 13 | 6 | 15 | 6 | 13 |
| Sample | DZ27 | DZ30 | DZ43 | DZ45 | DZ47 | DZ49 | DZ50 | DZ52 | DZ56 |
| Geological unit | OS | OBS | TT | MBV | TT | OS | TT | TT | OS |
| $SiO_2$ | 57.49 | 47.79 | 61.88 | 71.55 | 61.31 | 58.69 | 68.21 | 63.44 | 69.75 |
| $TiO_2$ | 2.06 | 3.50 | 1.40 | 0.52 | 0.83 | 1.49 | 0.60 | 0.75 | 0.33 |
| $Al_2O_3$ | 18.03 | 17.71 | 17.71 | 14.91 | 18.29 | 17.58 | 16.57 | 18.51 | 15.74 |
| $FeO_{tot}$ | 7.41 | 10.53 | 3.40 | 3.95 | 3.26 | 6.01 | 2.66 | 3.61 | 2.51 |
| MnO | 0.19 | 0.16 | 0.08 | 0.11 | 0.15 | 0.19 | 0.05 | 0.08 | 0.20 |
| MgO | 1.83 | 4.53 | 1.05 | 1.40 | 0.49 | 1.23 | 0.19 | 0.53 | 0.19 |
| CaO | 3.40 | 9.72 | 3.39 | 1.55 | 3.27 | 4.39 | 0.22 | 0.51 | 0.39 |
| $Na_2O$ | 4.90 | 2.95 | 4.86 | 4.35 | 5.69 | 4.84 | 4.86 | 4.83 | 5.09 |
| $K_2O$ | 3.90 | 2.26 | 5.79 | 1.51 | 6.50 | 4.99 | 6.51 | 7.56 | 5.75 |
| $P_2O_5$ | 0.79 | 0.85 | 0.45 | 0.15 | 0.22 | 0.59 | 0.13 | 0.18 | 0.04 |
| TOT | 100.00 | 100.00 | 100.00 | 100.00 | 100.00 | 100.00 | 100.00 | 100.00 | 100.00 |
| $H_2O^-$ | 0.24 | 0.59 | 0.32 | 0.53 | 0.14 | 0.20 | 0.25 | 0.40 | 0.28 |
| LOI | 1.31 | 0.44 | 0.65 | 2.29 | 1.99 | 1.33 | 1.19 | 0.84 | 0.66 |
| Sc | 13 | 26 | 9 | 8 | 9 | 11 | 3 | 4 | 2 |
| V | 122 | 268 | 57 | 35 | 18 | 62 | 16 | 19 | 6 |

**Table 1** continued

| Sample | DZ27 | DZ30 | DZ43 | DZ45 | DZ47 | DZ49 | DZ50 | DZ52 | DZ56 |
|---|---|---|---|---|---|---|---|---|---|
| Geological unit | OS | OBS | TT | MBV | TT | OS | TT | TT | OS |
| Cr | 4 | 4 | 4 | 4 | bdl | bdl | bdl | bdl | bdl |
| Co | 15 | 29 | 3 | 6 | 3 | 6 | 3 | 3 | 2 |
| Ni | 10 | 12 | 7 | 7 | 4 | 1 | 7 | 5 | 7 |
| Cu | 2 | 13 | 8 | 7 | 8 | 3 | 8 | 4 | 6 |
| Zn | 105 | 94 | 117 | 54 | 76 | 110 | 69 | 99 | 179 |
| Ga | 23 | 22 | 23 | 15 | 23 | 23 | 23 | 26 | 30 |
| Rb | 89 | 58 | 128 | 65 | 111 | 119 | 206 | 214 | 210 |
| Y | 37 | 26 | 36 | 40 | 31 | 37 | 49 | 39 | 72 |
| Sr | 847 | 944 | 566 | 340 | 293 | 696 | 169 | 196 | 16 |
| Zr | 467 | 253 | 621 | 286 | 786 | 456 | 800 | 933 | 887 |
| Nb | 88 | 54 | 84 | 9 | 84 | 88 | 111 | 75 | 162 |
| Ba | 1783 | 770 | 1455 | 516 | 995 | 1854 | 629 | 1354 | 49 |
| Pb | 12 | 6 | 14 | 10 | 17 | 17 | 14 | 15 | 20 |
| La | 103 | 61 | 96 | 36 | 99 | 98 | 114 | 85 | 185 |
| Ce | 286 | 145 | 249 | 86 | 221 | 277 | 244 | 215 | 319 |
| Th | 14 | 8 | 14 | 8 | 14 | 12 | 21 | 13 | 34 |

*bdl* Below detection limit

Geological units: *OS* Ōyama syenite, *TT* Takuhiyama trachyte, *UB* Uzuka basalt, *DT* dispersed trachytes, *OBS* outer basaltic succession, *MBV* Miocene basement volcanics

About 50 mg sample powder was digested with HF, $HClO_4$ and $HNO_3$. After the digestion, the solution was evaporated to dryness and dissolved in 7 M $HNO_3$. The solution was passed through a plastic column filled with 0.5 ml of Sr resin (Sr Resin, particle size, 50–100 μm, Eichrom Technologies, Inc.). The resin was cleaned with 7 M $HNO_3$. Nd was passed through the column with major elements in this fraction. Sr and Pb were sequentially separated with 0.4 M $HNO_3$ and 9 M HCl, respectively. Rare earth elements were separated from major elements in the Nd fraction by using conventional cation exchange column using DOWEX AG50 W-X8. Nd was separated from other rare earth elements with Ln resin (Ln Resin, particle size, 100–150 μm, Eichrom Technologies, Inc.). Procedural blanks were <30 pg/g for both Nd and Sr. Procedural blank for Pb was typically <100 pg. NIST SRM987 Sr standard was analysed before and after each 3 unknowns. Measured $^{87}Sr/^{86}Sr$ ratios of unknowns were normalized by NIST SRM987 using normalizing value of $^{87}Sr/^{86}Sr = 0.710258$. Typical reproducibility of $^{87}Sr/^{86}Sr$ analysis on NIST SRM987 was ±0.000023 ($n = 5$, errors in $2\sigma$). JNdi-1 standard was analysed before and after each 3 unknowns. Standard values during the analyses was $^{143}Nd/^{144}Nd = 0.512141 \pm 0.000027$ ($n = 4$, errors in $2\sigma$). Typical internal 2 standard errors for sample analyses were ±0.000014 for Sr and ±0.000010 for Nd. During Pb isotope analyses, mass fractionation factors were corrected using a Tl external standard. NIST SRM981 Pb standard was analysed before and after each 3 unknowns. Measured Pb isotope ratios of unknowns were normalized by NIST SRM981 using normalizing values of $^{206}Pb/^{204}Pb = 16.9416$, $^{207}Pb/^{204}Pb = 15.4999$ and $^{208}Pb/^{204}Pb = 36.7259$ (Baker et al. 2004). Reproducibility of NIST SRM981 analyses was ±0.0052 for $^{206}Pb/^{204}Pb$, ±0.0061 for $^{207}Pb/^{204}Pb$ and ±0.018 for $^{208}Pb/^{204}Pb$ ($n = 5$). Typical in-run precisions were ±0.0008 for $^{206}Pb/^{204}Pb$, ±0.0008 for $^{207}Pb/^{204}Pb$ and ±0.0020 for $^{208}Pb/^{204}Pb$. Analytical results are reported in Table 2.

Zircon U–Pb dating was performed using laser-ablation inductively coupled-plasma mass-spectrometry (LA-ICP-MS). The dating procedures were analogous to those described in Ito (2014) except that zircons were not polished and 40 μm laser beam with fluence of 4–6 J/cm$^2$ was used. The accuracy and precision of the age data were confirmed by analysis of standard OD-3 (Iwano et al. 2013), which was also dated using unpolished zircons. Full details of the analytical results are presented in Electronic Appendix 3.

## Geology, petrography and mineral chemistry

We collected samples from all main eruptive units at Oki-Dōzen. The focus of this study is on the central portion of the volcanic system including the Takuhiyama trachyte and the associated Ōyama syenite. Brief descriptions will also be given for the outer (somma) basaltic rocks and the dispersed trachytes.

**Table 2** Sr–Nd–Pb isotope data for Oki-Dōzen samples

| Sample | $^{87}Sr/^{86}Sr$ | $^{87}Sr/^{86}Sr_i$ | $^{143}Nd/^{144}Nd$ | $^{206}Pb/^{204}Pb$ | $^{207}Pb/^{204}Pb$ | $^{208}Pb/^{204}Pb$ |
|---|---|---|---|---|---|---|
| DZ02S | 0.710428 | 0.710094 | 0.512459 | 17.88 | 15.57 | 38.99 |
| DZ03 | 0.711883 | 0.711413 | 0.512483 | 17.94 | 15.58 | 39.09 |
| DZ06 | 0.710309 | 0.710173 | 0.512473 | 17.94 | 15.57 | 39.05 |
| DZ15 | 0.706260 | 0.706251 | 0.512697 | 18.02 | 15.56 | 38.51 |
| DZ20 | 0.706090 | 0.706023 | 0.512516 | 17.91 | 15.56 | 39.02 |
| DZ43 | 0.706119 | 0.706066 | 0.512489 | 17.94 | 15.57 | 39.13 |
| DZ45 | 0.708589 | 0.708475 | 0.512430 | 18.31 | 15.61 | 38.95 |
| DZ49 | 0.706173 | 0.706137 | 0.512502 | 17.87 | 15.56 | 39.03 |
| DZ52 | 0.706536 | 0.706279 | 0.512521 | 17.93 | 15.56 | 39.03 |
| DZ56 | | | | 17.92 | 15.54 | 39.00 |

Standard errors are reported in the "Analytical procedures" section

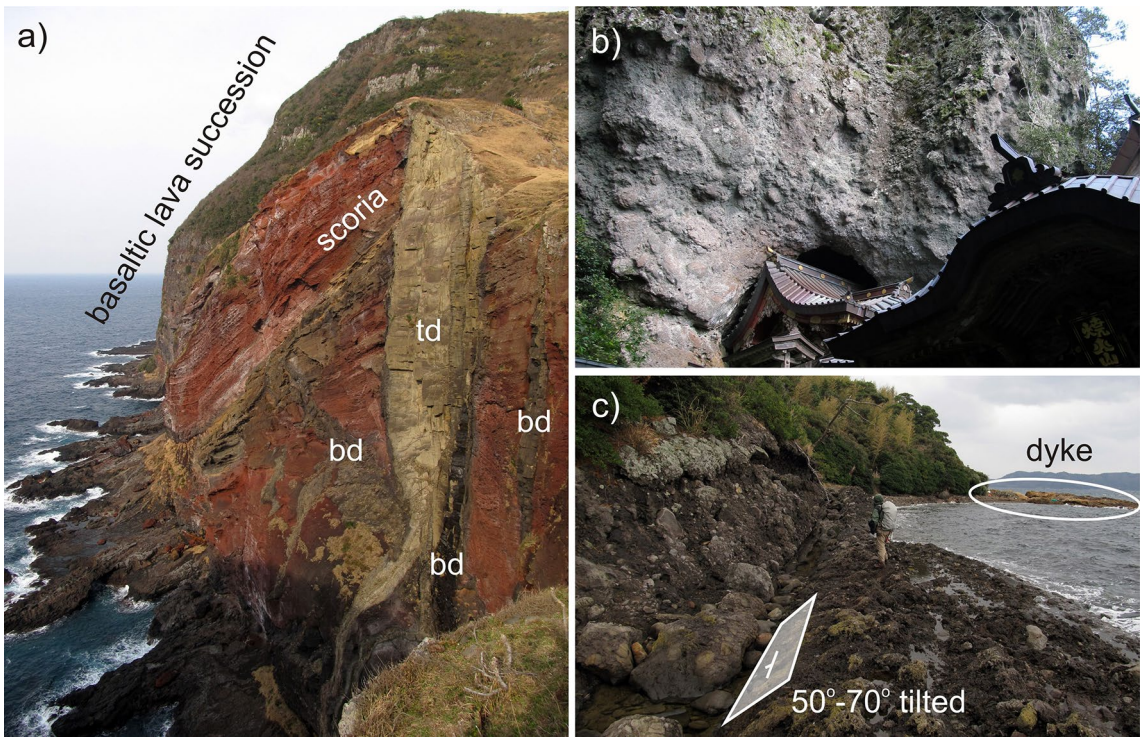


**Fig. 2** **a** Dissected scoria cone within the outer basaltic lava succession, which was later intruded by basaltic (*bd*) and trachytic (*td*) dykes. **b** Volcaniclastic unit close to the summit of Takuhiyama. *Note* The subrounded boulder surfaces and preferentially weathered matrix, which highlights boulder shapes. **c** Volcanic breccia on the south-western shore of Takuhiyama. This unit overlies a sequence of bedded (locally cross-bedded) coarse sandstone to conglomerate with finer silty horizons. The units are uniformly tilted 50–70°NE. *Note* The *pale orange* competent unit (dyke) in the background

## Flank basaltic volcanism—outer edifice

Samples were collected from lava flows belonging to the "somma" (hereafter termed "outer flank") volcanic phase as well as from the younger Uzuka scoria cone and basalt flows (Fig. 1c). The former occur as generally <5-m-thick lava flows in a succession including autobreccias and soil horizons, as well as dispersed pyroclastic deposits. Several dykes intrude and cross cut the succession and occasionally grade into dispersed vent areas, with dissected pyroclastic/scoria cones (Fig. 2a). The succession reaches elevations of 200–300 m. A drill-core intersected the basal contact c. 350 m below sea level (Kano et al. 2014), and hence, the maximum lava succession thickness is c. 600 m. The Uzuka scoria cone is a relatively well-preserved volcanic edifice on the eastern side of Nakanoshima, consisting of weakly aggregated spatter and scoria associated with a lava flow to the west (Fig. 1c).

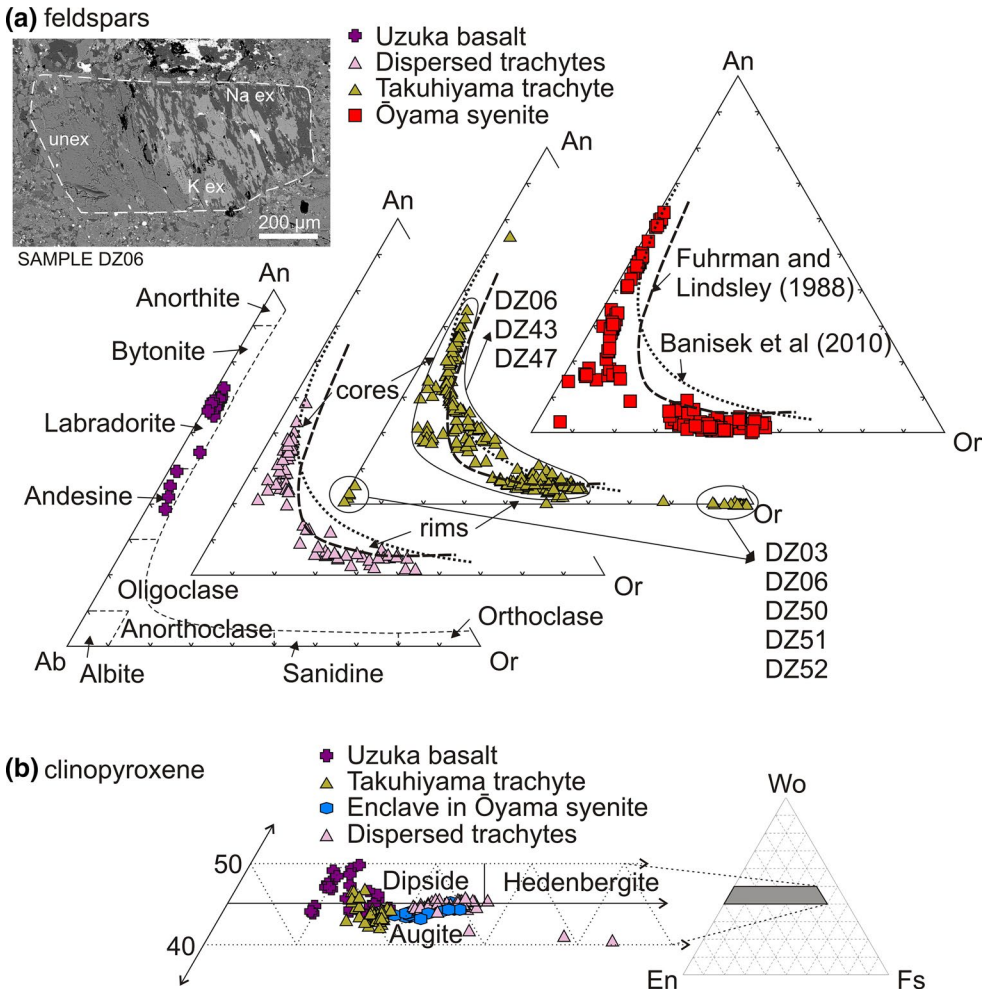


**Fig. 3** **a** Compositions of feldspars in Oki-Dōzen rocks. *Note* In the Takuhiyama trachyte feldspars are mostly exsolved in the samples proximal to the contact with the Ōyama syenite. The 900 °C isotherm *lines* are from Benisek et al. (2010) and Fuhrman and Lindsley (1988) and are provided for reference (quantitative temperature determination are done *below*). The *inset* shows the scanning electron microscope (SEM) back-scattered electron (BSE) image of a crystal from sample DZ06 partially exsolved to albite (Na ex) and orthoclase (K ex), as well as the retained unexsolved portion (unex). **b** Compositions of clinopyroxene from Oki-Dōzen

The basaltic rocks contain variable amounts of phenocrysts (1–3 mm long) that are typically olivine + clinopyroxene ± feldspar set in a glassy (±altered) to clinopyroxene + feldspar + oxide microphyric groundmass. Olivine phenocrysts are generally subhedral and range in composition from $Fo_{88}$ in cores to $Fo_{76}$ on rims; groundmass olivine is generally $Fo_{74–84}$. In the outer flank rocks olivine crystals often show orange staining alteration/hydration. Feldspar phenocrysts in the Uzuka basalt are generally subhedral and have composition $An_{65–75}Ab_{25–35}Or_{<5}$ (Fig. 3a), whereas clinopyroxenes are diopsidic ($Wo_{44–50}En_{38–46}Fs_{9–16}$; Fig. 3b).

## Dispersed trachytes

The dispersed trachytic rocks have previously been separated into "mafic" and "felsic" groups (Tiba et al. 2000). The contacts of these bodies with their surrounding rock units are not well exposed, and it is therefore unclear whether these represent lava flows/domes or sub-volcanic intrusions, such as cryptodomes, sills or dome-feeding conduits. Tiba et al. (2000) mapped some tuffs underlying trachytic bodies suggesting an extrusive origin for, at least, some of these. The trachytes are often intruded by later basaltic dykes.

Samples representative of the relatively evolved trachytes are generally aphyric and consist of microcrystalline (<0.5 mm) feldspar with feldspar + biotite microphenocrysts up to 1 mm in size. The "mafic" trachyte (i.e. trachyandesite) samples contain feldspar + clinopyroxene + biotite ± amphibole phenocrysts (2–7 mm) in a fine flow-textured (trachytic) feldspar + oxides groundmass. Clinopyroxenes are diopsidic to augitic (Fig. 3b). Feldspar phenocryst compositions range widely between $An_{5–25}Ab_{30–55}Or_{10–50}$ with more An rich cores and more Or rich rims and a relative gap of Ab-rich (ternary solution) compositions (Fig. 3a).

## Central cone (Takuhiyama) trachyte

The central portion and highest part of Oki-Dōzen is Takuhiyama. This consists of a succession of trachyte

breccias and tuffaceous flow units (Tiba et al. 2000; Fig. 2b). No basaltic flows are sandwiched between the early Miocene sediments and the Takuhiyama trachyte, and the latter is not visibly intruded by basaltic dykes that are ubiquitous elsewhere on Oki-Dōzen (Tiba et al. 2000; Toshida et al. 2006). Near the subvertical contact between the Takuhiyama trachyte and Ōyama syenite, the brecciated units consist of generally sub-angular (cm to >m? scale) fragments in a dusty clay altered (devitrified/silicified?) matrix. Clasts within these breccias and tuffaceous units are generally crystal-rich and often contain fragmented crystals.

The slopes on the western side of Takuhiyama are skirted by volcano-sedimentary units that vary from coarse sandstone to conglomerate and breccia (Fig. 2c). The latter rocks are dominated by coarse angular clasts of trachytic textures that resemble those forming Takuhiyama. There are also minor basaltic/trachybasaltic clasts. Units are generally matrix-supported, although the coarser breccias are clast-supported. In the lower part, the sequence consists of bedded coarse sandstone that coarsens upward into a massive conglomerate unit containing boulders with diameters of up to ~1 m. The sequence then alternates between fine sandstone and coarser breccia/conglomerate that vary in thickness from several dm to m. Thick (in the order of m) monomict breccia units become prevalent further up the sequence. The sequence could not be followed to its top due to lack of access and exposure. The whole sequence is tilted 50°–70° towards the north-east (Fig. 2c). It is locally sheltered from wave action by vertically banded trachytic units (dykes? Fig. 2c).

Trachyte samples from Takuhiyama contain mainly feldspar + clinopyroxene phenocrysts ± biotite microphenocrysts and crystal fragments. Mafic crystals are often altered to chlorite and dusty clay minerals, particularly in samples collected near the contact with the syenite. Apatite, zircon, monazite, Fe–Ti oxides and sulphides are disseminated. Crystals are generally fragmented or anhedral but euhedral pyrite is locally abundant. Feldspar compositions are variable. Feldspars in a competent flow unit on the south-western flanks of Takuhiyama (DZ06) have compositions $An_{<10}Ab_{45–55}Or_{40–50}$ and show partial exsolution to albite and orthoclase (Fig. 3a inset). Feldspars collected on the north-eastern side of Takuhiyama near the contact with the syenite tend to have complete perthite exsolution, with analyses giving either $Ab_{>95}$ or $Or_{>90}$. Trachyte clasts from breccia units skirting Takuhiyama (DZ43 and DZ47) are the least altered, have feldspar with the largest ternary solid solution (i.e. $An_{20}Ab_{60}Or_{20}$; Fig. 3a) and do not show perthite exsolution, but some crystals have resorbed cores. Other phases, including clinopyroxene and rare biotite, are not altered in the latter units, which also lack pyrite. Clinopyroxene is diopsidic to augitic ($Wo_{42–47}En_{38–41}Fs_{12–18}$; Fig. 3b).

### Ōyama syenite

The syenite body is exposed in the central part of Nishinoshima (Fig. 1c). Intrusive contacts with the pre-Oki early to middle Miocene volcano-sedimentary sequence are not well exposed, but Tiba et al. (2000) reported a few hundred-metre-wide hornfels zone of contact metamorphism. The contact with the Takuhiyama trachyte, exposed in a road cut near the saddle between Ōyama and Takuhiyama, is subvertical and sharp without crystal size reduction or chilled margins. This contact extends subvertically from the north-eastern slope of Takuhiyama towards the bottom of the valley. The intrusive body is locally cut by aplitic veins and contains dm-scale enclaves of a fine-grained, darker rock. Samples were collected at various localities, where the rock texture and colour are slightly variable, and from the enclaves.

The syenite mainly consists of 5- to 10-mm feldspar crystals with interstitial (1–4 mm) amphibole + biotite + oxides. Mafic minerals modally vary between 5 and 15 %. Trace minerals include zircon, apatite and a La + Ce-rich phase identified as chevkinite. No feldspathoid minerals have been found, but quartz is present, often interstitially. Feldspar crystals are variably altered to dusty clay minerals especially along margins and cracks and have microperthitic exsolution that was interpreted to be the result of deuteric alteration (Nakano 1998). Feldspars in the relatively mafic crystal-poor rock have composition $An_{<8}Ab_{40–65}Or_{35–58}$, whereas feldspars in the relatively mafic crystal-rich rock have composition $An_{15–62}Ab_{35–75}Or_{<15}$ (Fig. 3a). Amphibole crystals are anhedral to subhedral with distinct cleavage and have composition of ferro-edenite following the classification of Leake et al. (1997). Amphibole is often altered and completely replaced by opaque minerals and mica.

The enclaves within the syenite consist of fine (<0.5 mm) interlocking augitic clinopyroxene (Fig. 3b) and feldspar crystals with interstitial oxides. Additionally, larger feldspar crystals akin to those constituting the syenite are contained within the enclave fine-grained material.

## Analytical results

### Whole-rock major and trace element geochemistry

The major element compositions of the analysed Oki-Dōzen samples form a relatively continuous spectrum from alkalic basalt to trachyte and rhyolite in agreement with previous

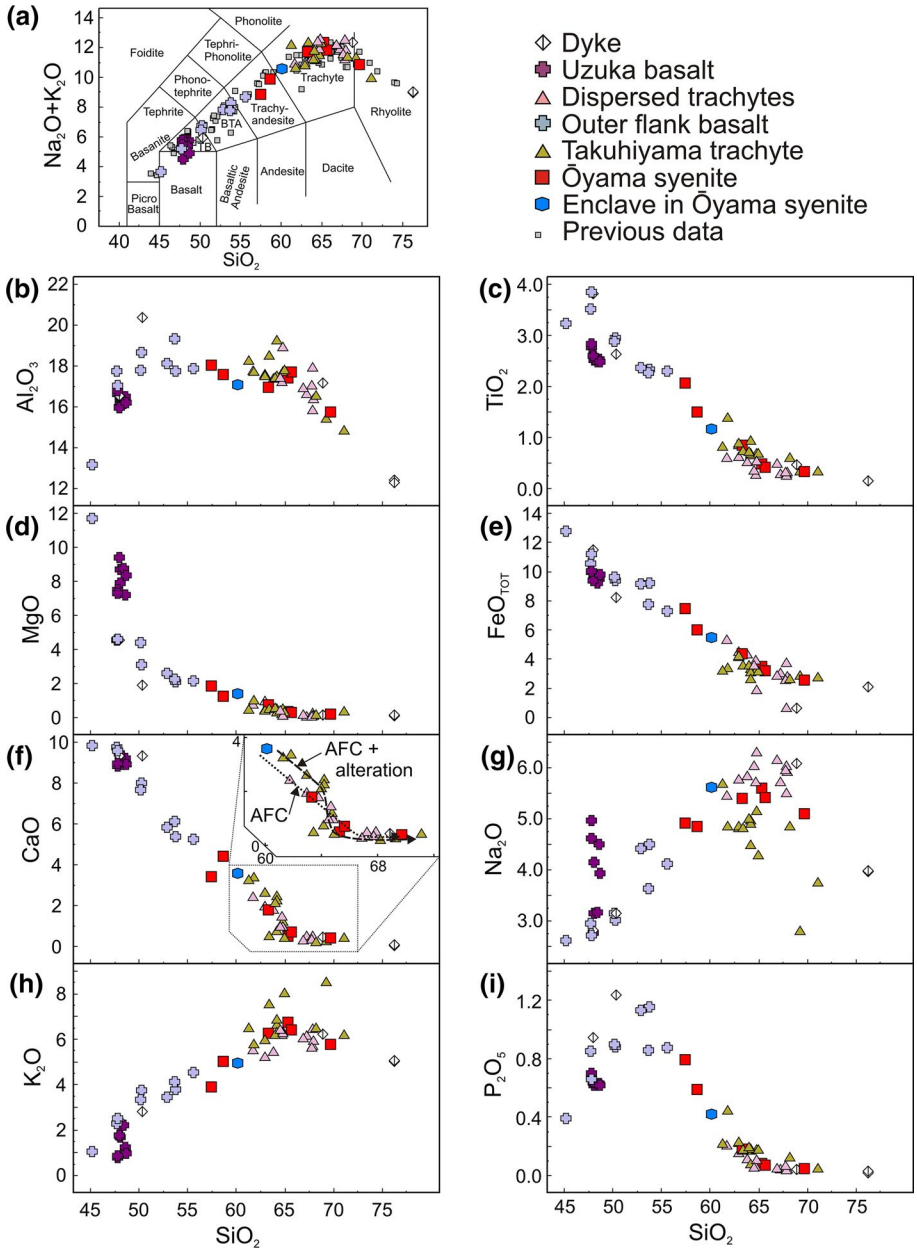


**Fig. 4** **a** Total Alkali versus Silica (TAS) diagram after LeBas et al. (1986) including a compilation of previous Oki-Dōzen data (Kaneko et al. 1983; Morris 1986; Tiba 1986; Morris and Kagami 1989; Wada et al. 1990; Kaneko 1991; Morris et al. 1997), which are consistent with our new measurements. TB is trachybasalt and BTA is basaltic trachyandesite. **b–i** Major element versus $SiO_2$ variation for the new data only. **f** Expected variation for assimilation and fractional crystallization (AFC) and AFC + alteration. See "Discussion" section for details

studies (Kaneko et al. 1983; Morris 1986; Tiba 1986; Morris and Kagami 1989; Wada et al. 1990; Kaneko 1991; Morris et al. 1997; Fig. 4a). The most frequent compositions of eruption products are, however, trachybasalt to basaltic trachyandesite, or trachyte. All samples belong to the alkalic suite.

The relatively more mafic end of the spectrum (c. 45–55 wt% $SiO_2$) is mainly represented by samples of the outer flanks of Oki-Dōzen. One eruptive centre sampled in greater detail is the Uzuka basaltic scoria cone and lava flow. Although the $SiO_2$ variation within this centre is relatively restricted (47.5–49 wt%), $Na_2O$ and $K_2O$ show strong changes (2.5 and 1.5 wt%, respectively), larger than in the remaining basaltic samples. Overall in the relatively mafic samples, $TiO_2$, FeO, MgO, MnO and CaO are negatively correlated with $SiO_2$, whereas $Al_2O_3$, $Na_2O$, $K_2O$ and $P_2O_5$ are positively correlated with $SiO_2$ (Fig. 4). $P_2O_5$ peaks around 54 wt% $SiO_2$ (Fig. 4i).

Trachytic to rhyolitic rocks (>60 wt% $SiO_2$) occur as single eruptive/intrusive bodies throughout Oki-Dōzen but are volumetrically more abundant in the centre (Takuhiyama). The trachytes were chemically distinguished into two groups based on $Na_2O$ and $K_2O$ concentrations (Morris et al. 1997). Those from Takuhiyama tend to have lower $Na_2O$ but higher $K_2O$ than those of the dispersed trachytes occurring on the outer flanks of the volcano (Fig. 4g, h). Tiba et al. (2000) introduced a distinction of "mafic" and "felsic" dispersed trachytes. Given the relative continuity of the chemical variation at Oki-Dōzen, we consider

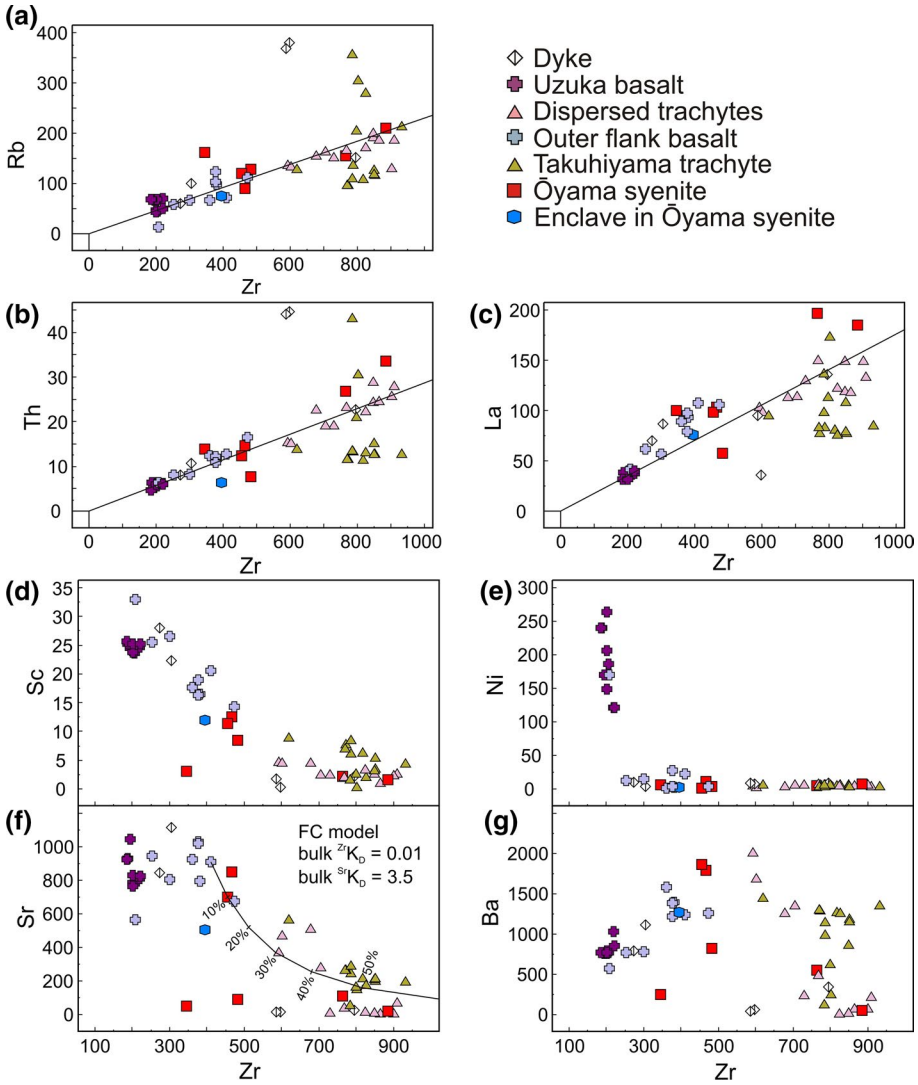


**Fig. 5** Trace element characteristics of Oki-Dōzen rocks. The *lines* through the origin and the more primitive samples in (**a**–**c**) illustrate the incompatibility of Rb, Th and La with respect to Zr. *Note* The different variation of these elements suggesting the influence of trace mineral phases (e.g. chevkinite, apatite), particularly in the Takuhiyama trachyte. The Rayleigh fractional crystallization (FC) model in (**f**) shows removal of percentage mineral volumes

dispersed trachytes as a single group, i.e. a continuation of the alkalic basalt-trachyandesite chemical trend observed in the rest of the outer flank lavas. Apart from $Na_2O$ and $K_2O$, all major elements in the trachytic samples are negatively correlated with increasing $SiO_2$. $K_2O$ has a weak positive correlation with $SiO_2$, and the Takuhiyama trachyte tends to form a $Na_2O$ depletion trend, as opposed to other trachytic samples from Oki-Dōzen.

Incompatible trace elements generally form a positive correlation with elements indicative of chemical evolution (e.g. Zr; Fig. 5a–c), particularly within the Uzuka basalt and flank lavas. However, the correlation is not continuous to the trachytic end of the chemical spectrum. In addition to their distinction in $Na_2O$ and $K_2O$ concentrations and variation trends, the Takuhiyama and dispersed trachytes also have different compatible and incompatible trace element characteristics. For instance, Th and La are depleted with respect to Zr in the Takuhiyama trachyte and plot below the incompatibility line projected through the origin and the most primitive alkalic basalt samples (Fig. 5a–c). At similar Zr content, the Takuhiyama trachyte samples have higher Sc, V, Sr and Ba compared to the dispersed trachytes (Fig. 5d–g). Likewise, the two Ōyama syenite samples with $SiO_2$ c. 58–60 wt% have higher Sc, V, Sr and Ba concentrations compared to the four samples with $SiO_2$ > 63 wt% despite two of the latter exhibiting comparable Zr contents. Ni and Cr are almost completely removed from the Oki-Dōzen samples, apart for the Uzuka basalt, which has a relatively broad range of concentrations from c. 100 to 300 ppm (Fig. 5e).

## Sr–Nd–Pb isotopes

Twelve samples representative of different intrusive and eruptive units of Oki-Dōzen were analysed for Sr, Nd and Pb isotopic compositions (Table 2; Fig. 6). $^{87}Sr/^{86}Sr$ and $^{143}Nd/^{144}Nd$ data are analogous to those previously determined by Morris and Kagami (1989; Fig. 6a). The

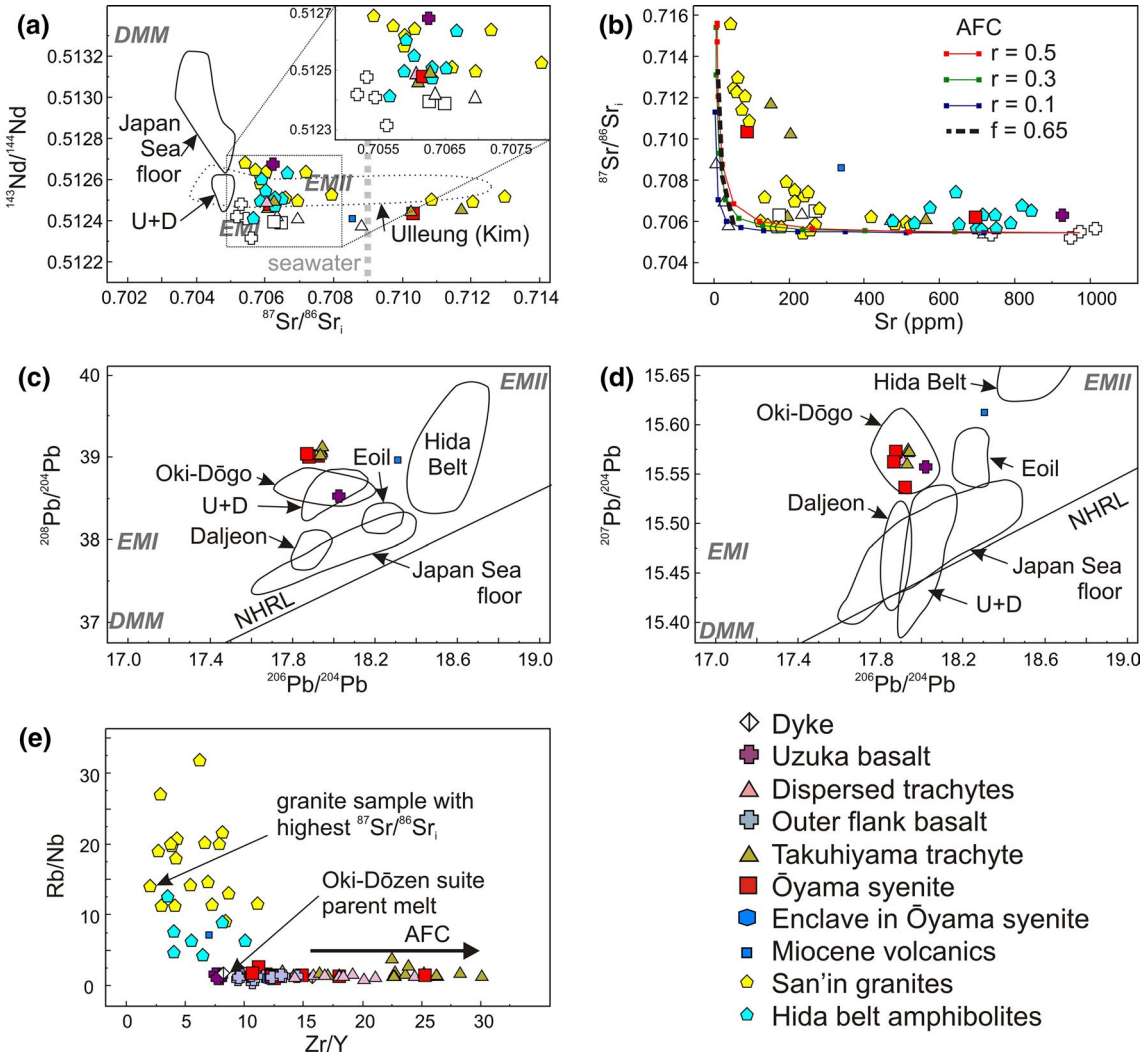


**Fig. 6** Sr–Nd–Pb isotopic variation of Oki-Dōzen rocks. **a** *Note* The large variation of $^{87}Sr/^{86}Sr_i$ ratio but relatively unchanged $^{143}Nd/^{144}Nd$ ratio of Oki-Dōzen rocks, similar to that of San'in Cretaceous granites of Kagami et al. (1992) as well as the variation of sea-water altered volcanic rocks from Ulleung (Kim et al. 1999). Open symbols are data from Morris and Kagami (1989). Hida belt amphibolite data are from Arakawa et al. (2000), Japan Sea data from Cousens et al. (1994), Ulleung and Dokdo (U + D) data from Brenna et al. (2014) and Tatsumoto and Nakamura (1991), seawater $^{87}Sr/^{86}Sr$ ratio is from Hodell et al. (1990). **b** Assimilation fractional crystallization (AFC) models with bulk Sr distribution coefficient taken as 3.5, three model lines with *r* (ratio of fractionated to assimilated volume) 0.1, 0.3 and 0.5, and the fractionation amount *f* shown in 10 % solid volume removed steps, with 65 % solid volume removed highlighted (*dashed line*). **c** $^{208}Pb/^{204}Pb$ versus $^{206}Pb/^{204}Pb$ and **d** $^{207}Pb/^{204}Pb$ versus $^{206}Pb/^{204}Pb$ of Oki-Dōzen rocks. *Note* The similarity with the field of Oki-Dōgo compositions (Kurasawa 1968). Tertiary Daljeon and Eoil basalt fields related to the opening of the Sea of Japan are from Choi et al. (2013). Ulleung and Dogdo (U + D) and the Japan Sea floor are the same as in (**a**). DMM, EMI and EMII in (**a**, **c**) and (**d**) are from Zindler and Hart (1986). The NHRL in (**c**) and (**d**) are from Hart (1984). **e** Trace element characteristics of Oki-Dōzen suite rocks, Cretaceous granites in the San'in region (Kagami et al. 1992) and Hida Belt amphibolite (Arakawa et al. 2000). The *AFC arrow* indicates the observed assimilation fractional crystallization direction, which is inconsistent with significant assimilation of crustal granite or amphibolite

$^{87}Sr/^{86}Sr$ was corrected to an initial ratio based on an age of 5.7 Ma for all the alkalic suite samples and an age of 2.8 Ma for the Uzuka basalt (Kaneko and Tiba 1998). The sample from the volcanic rocks of the early Miocene basement was corrected with an estimated age of 15 Ma. The $^{87}Sr/^{86}Sr_i$ of the Ōyama syenite and Takuhiyama trachyte varies from 0.706 to 0.712 (Fig. 6a) and extends the range of the data presented by Morris and Kagami (1989). The flanks basalt data by these authors have relatively lower $^{87}Sr/^{86}Sr_i$ (<0.706; Fig. 6a). The $^{143}Nd/^{144}Nd$ ranges from 0.5124 to 0.5125, well within the range of data of Morris and Kagami (1989). The Uzuka basalt stands out with a relatively higher $^{143}Nd/^{144}Nd$ ratio of 0.5127 (Fig. 6a).

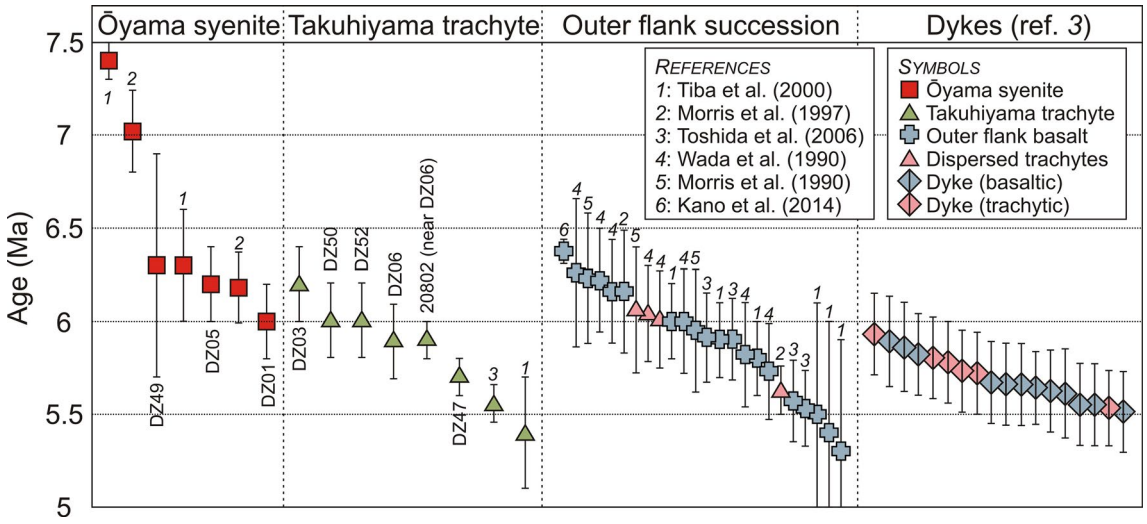


**Fig. 7** Newly determined zircon U/Pb ages for the Ōyama syenite and the Takuhiyama trachyte, and comparison with previously determined K/Ar ages [apart for Ar/Ar of Ref. Kano et al. (2014)] of these units and the outer flank basaltic to trachytic eruptive units and dykes. The Uzuka basalt (2.8 Ma; Kaneko and Tiba 1998) and a 2 Ma basalt boulder collected on the northern side of Nishinoshima (Tiba et al. 2000) were not included for clarity. *Error bars* are 2$\sigma$

The samples of the Oki-Dōzen alkalic suite have relatively homogeneous Pb isotopic characteristics. $^{206}Pb/^{204}Pb$, $^{207}Pb/^{204}Pb$ and $^{208}Pb/^{204}Pb$ show values of 17.8–18.1, 15.53–15.58 and close to 39, respectively, with the Uzuka basalt standing out with $^{208}Pb/^{204}Pb$ c. 38.5 (Fig. 6c). The sample from the early Miocene volcanics has distinct $^{206}Pb/^{204}Pb$ and $^{207}Pb/^{204}Pb$ compared to the alkalic suite samples. The Oki-Dōzen alkalic suite rocks and Uzuka basalt have Pb isotopic characteristics close to Oki-Dōgo volcanics (Kurasawa 1968) and the Ulleung and Dokdo volcanic systems (Tatsumoto and Nakamura 1991; Brenna et al. 2014), but are distinct from early Miocene (22–13 Ma) volcanic rocks from the Sea of Japan and the eastern margin of Korea (Cousens et al. 1994; Choi et al. 2013) or from metamorphic rocks of the Hida Belt (Miyazaki et al. 1973; Fig. 6c, d).

### Zircon ages

New zircon U/Pb ages for three Ōyama syenite and six Takuhiyama trachyte samples were determined and are illustrated in Fig. 7 with full analytical results reported in Electronic Appendix 3. Ōyama syenite zircons yielded ages of 6–6.3 Ma, and Takuhiyama trachyte zircons were dated at 5.7–6.2 Ma (Fig. 7). Previously determined K/Ar ages for these units (Morris et al. 1997; Tiba et al. 2000; Toshida et al. 2006) are generally within error of the new U/Pb ages, apart for one relatively older syenite age of 7.4 Ma (Tiba et al. 2000). Therefore, the new Ōyama syenite and Takuhiyama trachyte ages overlap with those of the outer basaltic and dispersed trachytic lava and dyke succession (Kano et al. 2014; Morris et al. 1997, 1990; Tiba et al. 2000; Toshida et al. 2006; Wada et al. 1990; Fig. 7).

## Discussion

### Magma source

The more primitive samples of the Oki-Dōzen alkalic suite have Ocean Island Basalt (OIB)-like trace element abundances (Fig. 8) and, excluding the Uzuka basalt, isotopic characteristics that suggest derivation from enriched mantle (EMI + EMII; Fig. 6). The younger Uzuka basalt has distinctly higher $^{143}Nd/^{144}Nd$ and lower $^{208}Pb/^{204}Pb$, and hence, it is more similar to the quaternary volcanic systems in the region (Oki-Dōgo, Ulleung, Dokdo; Fig. 6c, d), which, in addition to EMI + EMII, also bear a depleted MORB mantle (DMM) isotopic signature (Choi et al. 2006). Given its younger age and distinct isotopic characteristics, we consider the Uzuka basalt not to be consanguineously related to the earlier phase of alkalic activity of Oki-Dōzen.

Morris et al. (1997) recognized a distinction in trace element and isotopic characteristics between the central Takuhiyama trachyte + Ōyama syenite and the basaltic outer flanks with intercalated dispersed trachytes, and attributed this difference to derivation of the central magmas from partial melting of the lower crust after basaltic underplating. Crustal recycling was interpreted to have sourced the high $^{87}Sr/^{86}Sr$ Cretaceous granites in the San'in region (Kagami

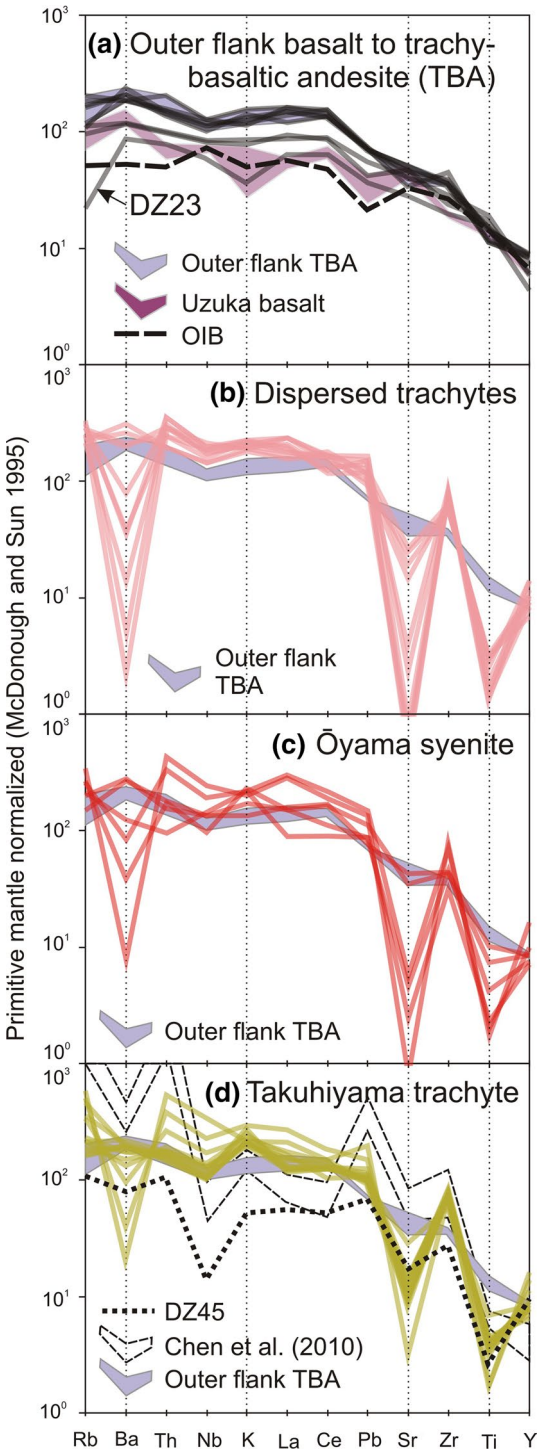


◀**Fig. 8** Primitive mantle (McDonough and Sun 1995) normalized diagram for the samples of the Oki-Dōzen alkalic suite. *a* Relatively primitive samples of the outer flanks. DZ23 is the most $SiO_2$ poor sample of the suite. OIB refers to the Ocean Island basalt of Sun and McDonough (1989). *b* Dispersed trachytes are relatively enriched, apart from depletions in Ba, Sr and Ti. *c* The Ōyama syenite has a range of enrichments and depletions from the more primitive to more evolved samples. *d* The Takuhiyama trachyte samples have a range of element enrichments and depletions. DZ45 represents the Miocene basement volcanic rocks. The Chen et al. (2010) field refers to rocks interpreted as the result of lower crustal melting processes

et al. 1992). We consider re-melting of the source that produces the San'in granites unlikely because of the consistent OIB-like trace element abundance (e.g. Nb, Rb, Zr and Y; Weaver 1991) of the Oki-Dōzen suite (basalt to trachyte/syenite) compared to the San'in granites (Kagami et al. 1992; Fig. 6e). The first melting episode in the Cretaceous would have already depleted the source in these elements. Partial melting of a different lower crustal granulite source, such as the Hida metamorphic belt, which forms part of the basement of the Oki Islands (Ishizaka and Yamaguchi 1969; Takahashi 1978), is also unlikely because its trace element and Pb isotopic characteristics are closer to EMII (Miyazaki et al. 1973; Arakawa et al. 2000; Kim et al. 2003; Fig. 6c, d). The slightly more radiogenic Pb isotope compositions of the Takuhiyama trachyte ($^{206}Pb/^{204}Pb = 17.93–17.94$; $^{208}Pb/^{204}Pb = 39.03–39.13$) compared to the Ōyama syenite ($^{206}Pb/^{204}Pb = 17.87–17.92$; $^{208}Pb/^{204}Pb = 38.99–39.03$; Table 2) are not sufficient to justify crustal melting as a source for the Takuhiyama trachyte. Additionally, lower crustal melting of amphibolites yields tonalite/trondhjemite magmas (Rapp et al. 1991; Rushmer 1991) or potassic to ultrapotassic rocks with trace element characteristics such as strong Th and Pb positive anomalies distinct from those of the Oki-Dōzen suite (Chen et al. 2010; Fig. 8d). The trachyte/syenite core is older than, or coeval to, the basaltic activity (Fig. 7), and hence, it is unlikely to have formed as a consequence of the latter (i.e. basaltic underplating).

Most Oki-Dōzen rocks (basalt and trachyte/syenite) have $^{87}Sr/^{86}Sr$ between 0.705 and 0.707 (Fig. 6a), which is consistent with derivation from the asthenospheric mantle (Choi et al. 2006) with possible minor contamination/assimilation. Nevertheless, some syenite and trachyte samples have $^{87}Sr/^{86}Sr$ between 0.710 and 0.712 (Fig. 6a). Assimilation and fractional crystallization (AFC) may change the magma compositions. We modelled the variation expected if Oki-Dōzen basaltic magmas with $SiO_2$ 51.5 wt%, Sr 973.9 ppm and $^{87}Sr/^{86}Sr_i$ 0.70545 (Morris and Kagami 1989) assimilated continental crust, represented by the San'in granite with 45 ppm Sr and $^{87}Sr/^{86}Sr$ of 0.71560 (Kagami et al. 1992) as plotted in Fig. 6b. The model (DePaolo 1981; Petrelli et al. 2005) with different values of r (the ratio of assimilation and crystallization volumes) and a bulk $^{Sr}Kd$ of 3.5, which is consistent with the chemical variation after the onset of Sr depletion (Fig. 5f), fails to account for the composition of the high $^{87}Sr/^{86}Sr$ Oki-Dōzen samples. Although some contamination may be responsible for the slight to moderate increase in the $^{87}Sr/^{86}Sr$ seen in some of the Oki-Dōzen trachytes and syenites (Fig. 6a inset), we consider the process unlikely to have generated the samples with $^{87}Sr/^{86}Sr$ between 0.710 and 0.712.

### Hydrothermal alteration of the central complex

The anomalously high $^{87}Sr/^{86}Sr$ of these samples may alternatively be due to hydrothermal alteration. Such a process was proposed for volcanic rocks with similarly high $^{87}Sr/^{86}Sr$ at Ulleung Island (Kim et al. 1999, 2008; Fig. 6a) and Ascension Island (Sheppard and Harris 1985; Kar et al. 1998). The $^{87}Sr/^{86}Sr$ composition of seawater c. 6 Ma ago was c. 0.709 (Hodell et al. 1990) and therefore not high enough to cause the increased $^{87}Sr/^{86}Sr$ ratio of some Oki-Dōzen samples. It is nonetheless possible that some seawater infiltrated into the seafloor was contaminated by high $^{87}Sr/^{86}Sr$ sediments and basement rocks, and later interacted with the Oki-Dōzen magmatic system. As not all syenite and trachyte samples have high $^{87}Sr/^{86}Sr$, alteration did not occur in a magmatic reservoir, which may have homogenized $^{87}Sr/^{86}Sr$. It is therefore likely that alteration occurred in a surface hydrothermal system during eruption or shortly after it.

The chemical and petrographic characteristics of the Takuhiyama trachyte additionally point to this process having occurred. Calcium is mobile in hydrothermal fluids and in the absence of anhydrite precipitation (as is the case at Oki-Dōzen) may be depleted from the rock (Seyfried 1987; Gianelli and Grassi 2001; Fig. 4f). Takuhiyama trachyte samples collected close to the contact with the Ōyama syenite show complete feldspar perthite exsolution to albite and orthoclase (Fig. 3a). In volcanic rocks subsolidus feldspar exsolution does not generally occur because crystals cool rapidly (Parsons and Brown 1984). Most feldspars in the syenite do not generally show such chemical distinction (Fig. 3a), and it is therefore unlikely that the exsolved feldspar crystals in the Takuhiyama trachyte are fragments derived from the syenite body. Deuteric alteration by late-stage magmatic or hydrothermal fluids can nonetheless give rise to perthite exsolution in feldspars (Parsons and Brown 1984; Parsons and Lee 2009). Additionally, feldspars and groundmass are often altered to sericite and clay minerals, which can incorporate Rb (Berger et al. 1988), explaining its wide variability in the Takuhiyama trachyte (Fig. 5a). Disseminated pyrite also occurs in these samples, pointing to hydrothermal alteration. The hydrothermal process did not significantly affect the outer flank trachytic lavas because they are smaller in volume and hence would not have developed significant hydrothermal circulation.

### Fractional crystallization

Mantle-derived melts may ascend and erupt relatively unmodified, such as in many monogenetic basaltic eruptions or stall at various levels to evolve chemically through crystal fractionation. Several trachyte bodies were erupted at Oki-Dōzen, and even the more primitive basaltic rocks have mostly relatively low MgO, Ni and Cr concentrations (Figs. 4, 5), suggesting differentiation at crustal levels before eruption to the surface. Here we model this process by least squares calculations (Stormer and Nicholls 1978) performed with the software PetroGraph (Petrelli et al. 2005) based on mineral phases and whole-rock analyses. This modelling strategy is a simplification of the fractionation process based on constant mineral compositions and is independent of factors such as pressure and temperature. The results provide a semi-quantitative evaluation of the fractionating modal assemblage if the sum of the squared residuals (SSR) is <2 (Stormer and Nicholls 1978).

In order to overcome the model limitation, and given that different mineral assemblages fractionate at different degrees of magma evolution, we have divided the modelled compositions in four groups: (1) primitive basalt (DZ23, dyke) to trachybasalt (DZ24, lava), (2) trachybasalt (DZ24) to trachyandesite (DZ27), (3) trachyandesite (DZ27) to trachyte (DZ05) and (4) trachyte (DZ05) to rhyolite (DZ56). To represent the magmatic evolution within the plumbing system of the volcano, all samples apart from a lava flow (DZ27) are from intrusive units. The model input parameters and results are summarized in Electronic Appendix 4 and have SSR < 0.7. The low errors suggest that major and minor element variations within the Oki-Dōzen alkalic suite can be accounted for by crystal fractionation processes from a common alkalic basalt parent.

The Takuhiyama trachyte is distinctly poorer in $Na_2O$ and to a lesser extent richer in $K_2O$ compared to the Ōyama syenite and the dispersed trachytes (Fig. 4g, h). This distinction was previously employed by Morris et al. (1997) to argue for a crustal melting source of these rocks. Here we propose an alternative explanation for these geochemical differences.

The Takuhiyama trachyte crystallized feldspar compositions through a complete ternary solution series from the early-formed cores to the final rims (Fig. 3a), as opposed to the dispersed trachytes and Ōyama syenite, which have a compositional gap between the Ca-rich cores and the K-rich rims (Fig. 3a). Based on the experimental work of Nekvasil (1992), sodic feldspar crystallizes when $H_2O$ is not buffered by crystallization of hydrous phases, as is the case of the Takuhiyama trachyte. If $H_2O$ is instead buffered by crystallization of a hydrous phase (e.g. biotite, amphibole) during feldspar growth, the sodic molecule will not be incorporated into the crystal lattice and a gap will occur in the ternary feldspar plot, as seen for the dispersed trachytes and the Ōyama syenite (Fig. 3a). Here we estimate the water content of the silicic units using the melt-K feldspar hygrometer of Mollo et al. (2015). Equilibrium conditions are satisfied if the difference between measured and predicted feldspar-liquid orthoclase-albite distribution coefficient ($^{kfs-liq}Kd_{Or-Ab}$) is <0.1, but near-equilibrium conditions can be assumed when $\Delta\ ^{kfs-liq}Kd_{Or-Ab}$ <0.8 (Fig. 9a). These models are temperature

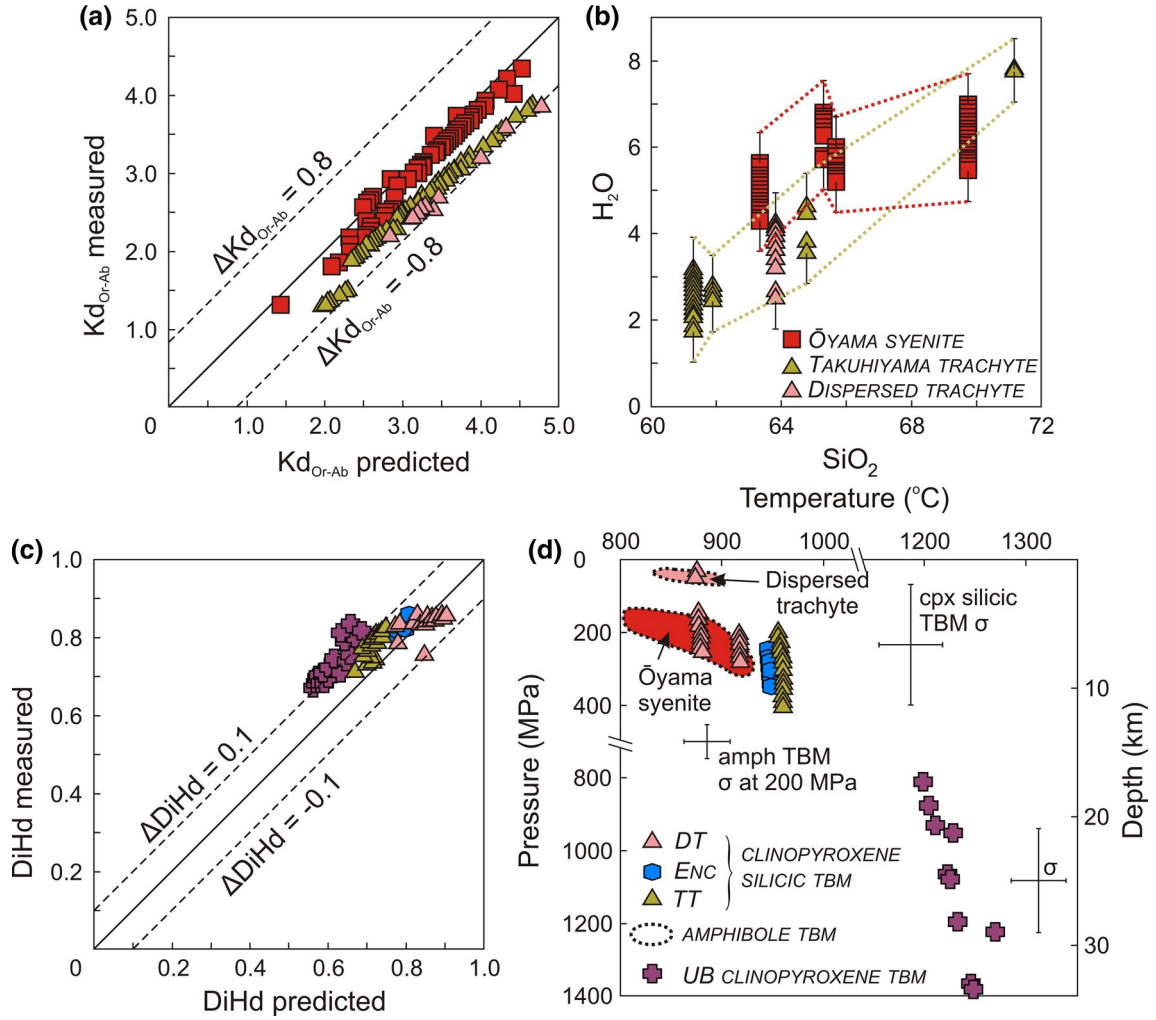


**Fig. 9** **a** Measured versus predicted $^{kfs-liq}Kd_{Or-Ab}$ in feldspars. **b** Results of the alkalic feldspar hygrometer of Mollo et al. (2015). **c** Measure of equilibrium based on predicted versus measured diopside + hedenbergite in clinopyroxene components (Mollo et al. 2013). **d** Results of thermobarometric models (TBM) described in the text. DT is dispersed trachyte, ENC is the trachytic enclave within the Ōyama syenite, TT is the Takuhiyama trachyte, UB is the Uzuka basalt

dependent. We used 950 °C for the Takuhiyama trachyte and 900 °C for the Ōyama syenite and dispersed trachyte, consistent with the thermometric models illustrated below (Fig. 9d). No exsolved feldspar compositions were used in the models. Results show that the Takuhiyama trachyte water content increases from c. 2–3 wt% at 61 wt% $SiO_2$ to c. 8 wt% at 71 wt% $SiO_2$ (Fig. 9b). In contrast, water content in the Ōyama syenite is more constant from c. 4–6 wt% at 63.5 wt% $SiO_2$ to c. 5–7 wt% at 70 wt% $SiO_2$ (Fig. 9b). The variations show that the Takuhiyama trachyte crystallized under water unbuffered conditions, whereas the Ōyama syenite crystallization was buffered by hydrous phases. The thermometric model below additionally illustrates that the Takuhiyama trachyte crystallized at higher temperature than the dispersed trachytes and Ōyama syenite. A high thermal condition may have suppressed the crystallization of amphibole and/or biotite. Indeed, biotite is rare in the Takuhiyama trachyte, whereas both biotite and amphibole are common in the dispersed trachytes and Ōyama syenite (Kaneko 1991). Depletion of Ba (and to a lesser extent K), which favourably partition into biotite (Villemant 1988), is seen in the dispersed trachytes and Ōyama syenite (Fig. 5g) and indicates that biotite was more greatly fractionated in these units compared to the Takuhiyama trachyte. We therefore conclude that the $Na_2O$ depletion in the Takuhiyama trachyte is due to crystallization and fractionation of sodic feldspar due to suppression of hydrous phases crystallization.

## Magma crystallization conditions

Crystallization pressure and temperature for clinopyroxene in the Uzuka basalt can be estimated using the

$H_2O$-independent thermobarometer of Putirka et al. (1996). This is valid for those crystals that are in near-equilibrium with their host basalt ($\Delta$DiHd $\leq$ 0.1) based on the calibration of Mollo et al. (2013), which relies on the predicted versus measured diopside + hedenbergite components in clinopyroxene. In the Uzuka basalt, clinopyroxene crystals are generally in disequilibrium with the whole-rock composition of their host because this contains a mafic crystal load that increases its Mg#. Near-equilibrium results can be attained for some crystals if these are modelled against the Uzuka basalt sample with the lowest Mg# (DZ10; Fig. 9c). Near-equilibrium crystals give modelled crystallization temperature of 1200–1280 ± 27 °C and pressures of 800–1400 ± 140 MPa (Fig. 9b). Further reducing the host Mg# would reduce estimated temperature and pressure, and hence, these results are to be considered maximum estimates. Although the Uzuka basalt is much younger, we consider these estimates representative of the crystallization conditions in the basaltic portion of the Oki-Dōzen alkalic suite, because they are consistent with results from other intraplate basaltic systems, such as those in Eastern Europe (Harangi et al. 2013).

The trachytic enclave within the Ōyama syenite and the Takuhiyama trachyte are estimated using the $H_2O$-independent model of Masotta et al. (2013). Clinopyroxene crystals in these units are mostly in near-equilibrium with the whole-rock composition of their host (Fig. 9c). The resulting temperature (Talk1) and pressure (Palk1) are 960 °C and 210–390 MPa for the Takuhiyama trachyte, 950 °C and 260–330 MPa for the trachytic enclave and 870–920 °C and 40–270 MPa for the dispersed trachyte (errors are ±32 °C and ±170 MPa; Fig. 9d).

Amphibole is present in the Ōyama syenite and the dispersed trachyte and its composition can be used with the amphibole thermobarometer of Ridolfi and Renzulli (2012), which is calibrated for alkalic systems. This model has relatively low uncertainties (±20 °C and ±50 MPa) and has been found to give reliable results in mildly alkaline magmas that contain only one type and simply zoned amphiboles (Kiss et al. 2014). Our predictions indicate that amphibole in the syenite crystallized at temperature of 800–900 °C and pressure of 100–300 MPa forming a pseudo-decompression path from higher to lower P–T conditions (Fig. 9d). These results are consistent with the crystallization pressure of clinopyroxene in the trachytic enclave within the syenite. Amphibole in the dispersed trachytes crystallized at similar temperature but shallower pressure (<50 MPa) consistent with the clinopyroxene thermobarometer results (Fig. 9d) and may therefore be the last products of crystallization shortly prior to eruption. These barometric results indicate that crystallization and differentiation occurred at a range of depths in the Oki-Dōzen plumbing system.

## Implications of the new zircon ages

As noted above, some discrepancies were found between the newly determined (older) U/Pb zircon and currently accepted (younger) K/Ar ages for the Takuhiyama trachyte samples. In the case of other volcanic settings, such discrepancies have been explained by previous authors (Schmitz and Bowring 2001; Bachmann et al. 2007) as due to the zircons having a long residence time in magma prior to eruption. However, we consider that the new U/Pb ages are a more accurate indication of the final crystallization and eruption age of the Takuhiyama trachyte. The thermobarometric estimates for the Takuhiyama trachyte suggest magmatic temperatures of c. 950 °C. The temperatures determined from the thermobarometric models were based on euhedral to subhedral clinopyroxene <2 mm in size, which do not show resorption textures. Such small crystals are unlikely to be residues from several hundreds of thousands of years of crystallization and therefore reliably represent the eruption temperature of the Takuhiyama trachyte. Magmatic temperatures of 900–1000 °C are consistent with other trachytic systems (Kuritani and Nakamura 2006; White et al. 2009; Masotta et al. 2013). This leads to the conclusion that it is unlikely that the U/Pb system in the Takuhiyama trachyte closed for hundreds of thousands of years prior to eruption (Lee et al. 1997). Additionally, zircon is considered to have relatively high solubility in alkaline magmas (Watson and Harrison 1983), and its crystallization tends to occur at the final solidification stage (Schmitt et al. 2010). This is supported by the lack of a Zr depletion trend in the Oki-Dōzen suite (Fig. 5). Assuming single intrusive and eruptive events, the new zircon crystal dating therefore constrains the age of the Takuhiyama trachyte to c. 5.9 Ma, which is shortly after the crystallization age of the Ōyama syenite at c. 6.2 Ma. This is older than the currently accepted K/Ar age of the Takuhiyama trachyte of c. 5.4 Ma (Tiba et al. 2000). The different ages for zircons within these units (as well as their different U content) may alternatively indicate their derivation from different magmatic injections, and hence a protracted magmatic/volcanic activity. The age-span of syenite (c. 1 Myr) and trachyte (c. 0.5 Myr) is of a similar magnitude to those of the outer succession (Fig. 7) and indicates that magmatism and volcanism were persistently supplied in both the central and outer parts of the system.

## Plumbing system model: "nest volcano"

At Oki-Dōzen the trachytic core (Takuhiyama) is surrounded by, but not underlain or intercalated with, basaltic lava flows that form the outer flanks of the volcano (Fig. 1). Basaltic dykes ubiquitous within the outer basaltic lava sequence do not intrude the early Miocene sediments

exposed to the north of Takuhiyama (Tiba et al. 2000), the Ōyama syenite or the Takuhiyama trachyte. The new zircon ages suggest that the Takuhiyama trachyte and Ōyama syenite were emplaced before or coevally to basaltic volcanism on the outer flanks (Fig. 7), but since these units are not intruded by basaltic dykes they are unlikely to have been covered by later basaltic eruptions. This points to the absence of the basaltic feeding system from the central portion of the Oki-Dōzen shallow magmatic system. Whole-rock major and trace elements and isotopic variability nevertheless suggest that all rock types, apart from the Uzuka basalt, belong to a single liquid line of descent originated from the same mantle-derived parental magma.

The Ōyama syenite is not a simple intrusion. It contains zircons that have some of the oldest ages in the Oki-Dōzen magmatic system (Fig. 7). Its whole-rock major and trace element compositions suggest at least four distinct chemical subsets: with 58–60, 63–66 and 70 wt% $SiO_2$, with in addition, samples DZ01 and DZ05 (63–66 wt% $SiO_2$ subset) having distinct Zr abundances. The U content of zircons in samples from the different subsets (e.g. DZ49 and DZ01; Electronic Appendix 3) differs by up to one order of magnitude. Therefore, the longevity (up to 1 Myr) of the Ōyama syenite together with its heterogeneous chemistry suggests that it does not represent crystallization of a magma reservoir generated by one single injection, but rather the input of several distinct magma batches in a shallow magma reservoir (Gudmundsson 2012). The formation of the trachytic enclave within the syenite may be directly related to the emplacement of a new magma batch derived from a deeper trachytic reservoir. Enclave formation follows fragmentation of a cooled dike by convection within the still partially molten syenite body (Andrews and Manga 2014). This may also explain why the enclave-hosting syenite sample has high $^{87}Sr/^{86}Sr$, as that portion of syenite would have been affected by magmatic and hydrothermal fluids related to the trachyte dyke emplacement episode.

The injection (within the syenite) of magma with trachytic rather than basaltic composition has implications for the plumbing system geometry at Oki-Dōzen. This relationship suggests the existence of smaller and differentiated reservoirs below the larger Ōyama syenite magma body. An array of secondary magma reservoirs at various depths in the central portion of the magmatic system may have acted as a filter for mantle-derived basaltic dykes. Such a complex plumbing system may explain why there are no basaltic lavas in the central portion of the volcano with later eruptions of trachytic magma forming the central cone (Takuhiyama trachyte). The higher temperature of the Takuhiyama trachyte (Fig. 9d) compared to the dispersed trachytes or the Ōyama syenite may indicate that it evolved in a more developed/mature plumbing system.

The Ōyama syenite does not represent a single magmatic reservoir extending beneath the whole island. Dispersed trachytes are erupted intercalated within the basaltic sequence of the outer flanks, which indicates that stalling and differentiation occurred also beyond the central portion of the plumbing system. These trachytic bodies are smaller than the central trachyte, and their dispersed nature did not constitute a hindrance for subsequent basaltic magmas rising towards the surface. The lesser degree of crystal volume removal by magmatic differentiation in the outer plumbing system implies that larger erupted volumes could build up a ring-shaped edifice, surrounding a volume-depleted (through AFC) core. A "nest-like", relatively primitive volcanic edifice was therefore formed around the central differentiated portion of the system.

## Significance for intraplate alkalic volcanism

North-east Asia is the site of current intraplate alkalic volcanic activity. Changbaishan (China/North Korea) has recently attracted scientific attention due to a seismic swarm beneath the volcano (Xu et al. 2012). Ulleung Island and Jeju Island (South Korea) were erupted during the Holocene and are therefore potentially still active. These three volcanoes display distinct chemical evolutionary trends. The Jeju Island magmatic system produced a continuous spectrum of compositions from alkalic basalt to trachyte, as well as some subalkalic flows (basalt to basaltic andesite) around the edges of the system (Brenna et al. 2012). At Ulleung Island, a single liquid line of descent produced alkalic basalt to trachytes followed by phonolites in the Holocene eruptions (Brenna et al. 2014). Changbaishan has a bimodal composition. A basaltic shield base is topped by a cone (Tianchi) of trachyte to pantellerite lava flows and ignimbrite units showing a chemical gap between 55 and 63 wt% $SiO_2$ (Liu et al. 1998).

Oki-Dōzen is similar to the aforementioned intraplate alkalic systems, but it is not entirely analogous to any of them. For instance, its chemical spectrum from alkalic basalt to trachyte lacks a marked "Daly Gap". The latter feature was interpreted at Changbaishan to indicate a bimodal storage system, with a deep (mantle) basaltic reservoir and a shallow (upper crust) rhyolitic reservoir (Liu et al. 1998). Such bimodal variability (Daly Gap) could alternatively be accounted for by the development and syn-eruptive collapse of a crystal mush in a shallow magma reservoir (Bachmann and Bergantz 2004; Dufek and Bachmann 2010; Masotta et al. 2010, 2012). The lack of such a distinction at Oki-Dōzen points to the absence of large catastrophic magma withdrawal and eruptions despite the presence of a shallow magmatic reservoir (Ōyama syenite). Indeed, petrographic and chemical evidence points to the presence of a number of vertically distributed (multi-stage;

Hansteen et al. 1998) magmatic reservoirs where primitive basaltic injections differentiated consecutively towards more trachytic compositions, rather than the formation and evolution of a single and large shallow magma reservoir (Bachmann et al. 2002). This would be akin to the shallow (upper crustal) version of a "hot zone" (Annen et al. 2006). Other volcanoes with multi-stage magma plumbing systems developed large conical edifices through centralized plumbing systems (Hansteen et al. 1998; Schwarz et al. 2004); however, Oki-Dōzen grew a nest-shaped volcano, possibly due to lower magma volumes and a more dispersed plumbing. Filtering by the multi-stage plumbing may have prevented the thermal destabilization of the shallower reservoir (Ōyama syenite). Indeed, large explosive eruptions are known to have been triggered by basaltic injections within differentiated magma reservoirs (Edgar et al. 2007; Shane et al. 2007; Wark et al. 2007). Additionally, a series of crustal reservoirs may have provided an opportunity for the ascending and differentiating magmas to re-equilibrate at new pressure conditions. Such a stepwise process may prevent explosive decompression (Eichelberger et al. 1986).

In regard to the source characteristics, at Jeju, primitive melts with alkalic (basanite) to subalkalic affinities formed in response to variable degrees of source partial melting at different depths due to an upwelling source (Tatsumi et al. 2005; Brenna et al. 2015). Instead, at Oki-Dōzen, both central and flank magmas were derived from a relatively homogeneous primitive alkalic basalt, which is indicative of a source within a vertically and laterally restricted portion of upper mantle. The primitive melt homogeneity also implies the homogeneity of melting degree and magma volume generation, which may explain why the core of the volcanic system appears "volume-depleted". Given the c. 2 Myr history of activity at Oki-Dōzen and constancy in chemical variability, the mantle source was relatively stable. This suggests a source melting mechanism other than continuous upwelling and decompression melting of peridotite and may be due to, for example, complex asthenospheric flow and regional tectonic reorganizations (Kimura et al. 2003, 2005).

## Conclusions

Between c. 7 and 5 Ma, the magmas at Oki-Dōzen evolved along a single liquid line of descent from an OIB-like alkalic basalt parent melt. The younger (2.8 Ma) basaltic centre (Uzuka basalt) represents a standalone eruption. Fractional crystallization and minor crustal assimilation processes resulted in the development of a syenitic and trachytic core surrounded by a ring-shaped sequence of basaltic to trachytic lava flows and interbedded eruptive centres. Basaltic products are absent from the core of the volcano because of the development of multiple (secondary) magma reservoirs that hindered the ascent of basaltic injections and prevented their surface emplacement. One of these solidified intrusive units is represented by the Ōyama syenite, whereas the composition of the central Takuhiyama trachyte testifies to the development of deeper reservoirs. The presence of a network of vertically separated crustal reservoirs preventing direct basaltic injections within the shallower differentiated reservoir may account for the lack of large explosive eruptions at Oki-Dōzen. Such a plumbing system may be a characteristic of differentiated volcanic systems dominated by effusive activity. The volcanic geology of Oki-Dōzen preserves a spectacular record of a variety of magmatic processes that can occur during formation of a small intraplate volcanic province.

**Acknowledgments** Nicola Jones helped with field logistics. Gabor Kereszturi provided the DEM image in Fig. 1 and Paul Morris kindly supplied a table of existing chemical analyses for Oki-Dōzen. The manuscript benefitted from discussion with Koji Kiyosugi, James White, Simon Barker and Manuela Tost. We are grateful to an anonymous reviewer and particularly to Silvio Mollo for providing a thorough review and detailed advice to improve the manuscript. Othmar Müntener is thanked for editorial handling. MB was supported by a visiting research fellowship from ERI, University of Tokyo.

## References

Andrews B, Manga M (2014) Thermal and rheological controls on the formation of mafic enclaves or banded pumice. Contrib Mineral Petrol 167:1–16. doi:10.1007/s00410-013-0961-7

Andújar J, Scaillet B (2012) Relationships between pre-eruptive conditions and eruptive styles of phonolite–trachyte magmas. Lithos 152:122–131. doi:10.1016/j.lithos.2012.05.009

Annen C, Blundy JD, Sparks RSJ (2006) The genesis of intermediate and silicic magmas in deep crustal hot zones. J Petrol 47:505–539. doi:10.1093/petrology/egi084

Arakawa Y, Saito Y, Amakawa H (2000) Crustal development of the Hida belt, Japan: evidence from Nd–Sr isotopic and chemical characteristics of igneous and metamorphic rocks. Tectonophysics 328:183–204

Bachmann O, Bergantz GW (2004) On the origin of crystal-poor rhyolites: extracted from batholithic crystal mushes. J Petrol 45:1565–1582

Bachmann O, Dungan MA, Lipman PW (2002) The Fish Canyon magma body, San Juan volcanic field, Colorado: rejuvenation and eruption of an upper-crustal batholith. J Petrol 43:1469–1503. doi:10.1093/petrology/43.8.1469

Bachmann O, Oberli F, Dungan MA, Meier M, Mundil R, Fischer H (2007) $^{40}Ar/^{39}Ar$ and U–Pb dating of the Fish Canyon magmatic system, San Juan volcanic field, Colorado: evidence for an extended crystallization history. Chem Geol 236:134–166. doi:10.1016/j.chemgeo.2006.09.005

Bachmann O, Deering C, Ruprecht J, Huber C, Skopelitis A, Schnyder C (2012) Evolution of silicic magmas in the Kos-Nisyros volcanic center, Greece: a petrological cycle associated with caldera collapse. Contrib Mineral Petrol 163:151–166. doi:10.1007/s00410-011-0663-y

Baker J, Peate D, Waight T, Meyzen C (2004) Pb isotopic analysis of standards and samples using a $^{207}Pb$–$^{204}Pb$ double spike and

thallium to correct for mass bias with a double-focusing MC-ICP-MS. Chem Geol 211:275–303
Benisek A, Dachs E, Kroll H (2010) A ternary feldspar-mixing model based on calorimetric data: development and application. Contrib Mineral Petrol 160:327–337. doi:10.1007/s00410-009-0480-8
Berger G, Schott J, Guy C (1988) Behavior of Li, Rb and Cs during basalt glass and olivine dissolution and chlorite, smectite and zeolite precipitation from seawater: experimental investigation and modelization between 50 and 300 °C. Chem Geol 71:297–312
Borley GD, Suddaby P, Scott P (1971) Some xenoliths from the alkalic rocks of Teneriffe, Canary Islands. Contrib Mineral Petrol 31:102–114. doi:10.1007/bf00373453
Brenna M, Cronin SJ, Smith IEM, Sohn YK, Maas R (2012) Spatiotemporal evolution of a dispersed magmatic system and its implications for volcano growth, Jeju Island Volcanic Field, Korea. Lithos 148:337–352. doi:10.1016/j.lithos.2012.06.021
Brenna M, Price R, Cronin SJ, Smith IEM, Sohn YK, Kim GB, Maas R (2014) Final magma storage depth modulation of explosivity and trachyte/phonolite genesis at an intraplate volcano: a case study from Ulleung Island, Republic of Korea. J Petrol 55:709–747
Brenna M, Cronin S, Kereszturi G, Sohn Y, Smith IM, Wijbrans J (2015) Intraplate volcanism influenced by distal subduction tectonics at Jeju Island, Republic of Korea. Bull Volcanol 77:1–16. doi:10.1007/s00445-014-0896-5
Chen J-L, Xu J-F, Wang B-D, Kang Z-Q, Jie L (2010) Origin of Cenozoic alkaline potassic volcanic rocks at KonglongXiang, Lhasa terrane, Tibetan Plateau: products of partial melting of a mafic lower-crustal source? Chem Geol 273:286–299. doi:10.1016/j.chemgeo.2010.03.003
Choi SH, Mukasa SB, Kwon ST, Andronikov AV (2006) Sr, Nd, Pb and Hf isotopic compositions of late Cenozoic alkali basalts in South Korea: evidence for mixing between the two dominant asthenospheric mantle domains beneath East Asia. Chem Geol 232:134–151
Choi H-O, Choi SH, Lee D-C, Kang H-C (2013) Geochemical evolution of basaltic volcanism within the tertiary basins of southeastern Korea and the opening of the East Sea (Sea of Japan). J Volcanol Geotherm Res 249:109–122
Cousens BL, Allan JF, Gorton MP (1994) Subduction-modified pelagic sediments as the enriched component in back-arc basalts from the Japan Sea: Ocean Drilling Program Sites 797 and 794. Contrib Mineral Petrol 117:421–434
DePaolo DJ (1981) Trace element and isotopic effects of combined wallrock assimilation and fractional crystallization. Earth Planet Sci Lett 53:189–202. doi:10.1016/0012-821x(81)90153-9
Diez M, Connor CB, Kruse SE, Connor L, Savov IP (2009) Evidence of small-volume igneous diapirism in the shallow crust of the Colorado Plateau, San Rafael Desert, Utah. Lithosphere 1:328–336. doi:10.1130/l61.1
Dufek J, Bachmann O (2010) Quantum magmatism: magmatic compositional gaps generated by melt-crystal dynamics. Geology 38:687–690. doi:10.1130/g30831.1
Edgar CJ et al (2007) The late quaternary Diego Hernandez formation, Tenerife: volcanology of a complex cycle of voluminous explosive phonolitic eruptions. J Volcanol Geotherm Res 160:59–85. doi:10.1016/j.jvolgeores.2006.06.001
Eichelberger JC, Carrigan CR, Westrich HR, Price RH (1986) Non-explosive silicic volcanism. Nature 323:598–602
Franz G et al (1997) The alkaline Meidob volcanic field (Late Cenozoic, northwest Sudan). J Afr Earth Sci 25:263–291. doi:10.1016/S0899-5362(97)00103-6
Fuhrman ML, Lindsley DH (1988) Ternary-feldspar modeling and thermometry. Am Mineral 73:201–215
Gianelli G, Grassi S (2001) Water-rock interaction in the active geothermal system of Pantelleria, Italy. Chem Geol 181:113–130
Gudmundsson A (2012) Magma chambers: formation, local stresses, excess pressures, and compartments. J Volcanol Geotherm Res 237–238:19–41. doi:10.1016/j.jvolgeores.2012.05.015
Hansteen TH, Klügel A, Schmincke H-U (1998) Multi-stage magma ascent beneath the Canary Islands: evidence from fluid inclusions. Contrib Mineral Petrol 132:48–64. doi:10.1007/s004100050404
Harangi S, Sági T, Seghedi I, Ntaflos T (2013) Origin of basaltic magmas of Perşani volcanic field, Romania: A combined whole rock and mineral scale investigation. Lithos 180–181:43–57. doi:10.1016/j.lithos.2013.08.025
Hart SR (1984) A large-scale isotope anomaly in the Southern Hemisphere mantle. Nature 309:753–757
Hodell DA, Mead GA, Mueller PA (1990) Variation in the strontium isotopic composition of seawater (8 Ma to present): implications for chemical weathering rates and dissolved fluxes to the oceans. Chem Geol 80:291–307
Ishizaka K, Yamaguchi M (1969) U–Th–Pb ages of sphene and zircon from the Hida metamorphic terrain, Japan. Earth Planet Sci Lett 6:179–185. doi:10.1016/0012-821X(69)90087-9
Ito H (2014) Zircon U–Th–Pb dating using LA-ICP-MS: simultaneous U–Pb and U–Th dating on the 0.1 Ma Toya Tephra, Japan. J Volcanol Geotherm Res 289:210–223. doi:10.1016/j.jvolgeores.2014.11.002
Iwano H et al (2013) An inter-laboratory evaluation of OD-3 zircon for use as a secondary U–Pb dating standard. Island Arc 22:382–394. doi:10.1111/iar.12038
Jellinek AM, DePaolo D (2003) A model for the origin of large silicic magma chambers: precursors of caldera-forming eruptions. Bull Volcanol 65:363–381. doi:10.1007/s00445-003-0277-y
Kagami H, Iizumi S, Tainosho Y, Owada M (1992) Spatial variations of Sr and Nd isotope ratios of Cretaceous-Paleogene granitoid rocks, Southwest Japan Arc. Contrib Mineral Petrol 112:165–177
Kaneko N (1991) Petrology of Oki-Dozen volcano. Part I. Petrography and major and trace element compositions. J Mineral Petrol Econ Geol 86:140–159
Kaneko N, Tiba T (1998) Occurrence and K–Ar age of an alkali olivine basalt from Nakanoshima in Oki-Dozen, Shimane Prefecture, Southwest Japan. J Geol Soc Japan 104:419–422
Kaneko N, Yoshida T, Aoki K (1983) Geochemical study of alkaline rocks from Oki Dozen islands, Shimane Prefecture. Research Report of the Laboratory of Nuclear Science, Tohoku University 16:151–159
Kano K, Kaneko N, Ishizuka O, Tiba T, Yanagisawa Y (2014) The beginning of lifetime of Dozen Volcano, Oki Islands, SW Japan. Bull Volcanol Soc Japan 59:77–88
Kar A, Weaver B, Davidson J, Colucci M (1998) Origin of differentiated volcanic and plutonic rocks from Ascension Island, South Atlantic Ocean. J Petrol 39:1009–1024. doi:10.1093/petroj/39.5.1009
Kim KH, Tanaka T, Nagao K, Jang SK (1999) Nd and Sr isotopes and K–Ar ages of the Ulreungdo alkali volcanic rocks in the East Sea, South Korea. Geochem J 33:317–341
Kim C-B, Chang H-W, Turek A (2003) U–Pb zircon ages and Sr–Nd–Pb isotopic compositions for Permian-Jurassic plutons in the Ogcheon belt and Ryeongnam massif, Korea: Tectonic implications and correlation with the China Qinling-Dabie belt and the Japan Hida belt. Island Arc 12:366–382. doi:10.1046/j.1440-1738.2003.00404.x
Kim KH, Nagao K, Sumino H, Tanaka T, Hayashi T, Nakamura T, Lee JI (2008) He–Ar and Nd–Sr isotopic compositions of late Pleistocene felsic plutonic back arc basin rocks from Ulleungdo volcanic island, South Korea: Implications for the genesis of

young plutonic rocks in a back arc basin. Chem Geol 253:180–195. doi:10.1016/j.chemgeo.2008.05.009

Kimura J-I et al (2003) Late Cenozoic volcanic activity in the Chugoku area, southwest Japan arc during back-arc basin opening and reinitiation of subduction. Island Arc 12:22–45. doi:10.1046/j.1440-1738.2003.00377.x

Kimura J-I, Stern RJ, Yoshida T (2005) Reinitiation of subduction and magmatic responses in SW Japan during Neogene time. Geol Soc Am Bull 117:969–986. doi:10.1130/b25565.1

Kiss B, Harangi S, Ntaflos T, Mason PD, Pál-Molnár E (2014) Amphibole perspective to unravel pre-eruptive processes and conditions in volcanic plumbing systems beneath intermediate arc volcanoes: a case study from Ciomadul volcano (SE Carpathians). Contrib Mineral Petrol 167:1–27. doi:10.1007/s00410-014-0986-6

Koh GW, Park JB, Kang BR, Kim GP, Moon DC (2013) Volcanism in Jeju Island. J Geol Soc Korea 49:209–230

Kurasawa H (1968) Isotopic composition of lead and concentrations of uranium, thorium, and lead in volcanic rocks from Dogo of the Oki Islands. Japan, Geochem J **2**

Kuritani T, Nakamura E (2006) Elemental fractionation in lavas during post-eruptive degassing: Evidence from trachytic lavas, Rishiri Volcano, Japan. J Volcanol Geotherm Res 149:124–138. doi:10.1016/j.jvolgeores.2005.06.008

Le Bas MJ, Lemaitre RW, Streckeisen A, Zanettin B (1986) A chemical classification of volcanic rocks based on the total alkali-silica diagram. J Petrol 27:745–750

Le Corvec N, Spörli KB, Rowland J, Lindsay J (2013) Spatial distribution and alignments of volcanic centers: clues to the formation of monogenetic volcanic fields. Earth-Sci Rev 124:96–114

Leake BE et al (1997) Nomenclature of amphiboles; report of the Subcommittee on Amphiboles of the International Mineralogical Association Commission on new minerals and mineral names. Mineral Mag 61:295–321

Lee JKW, Williams IS, Ellis DJ (1997) Pb, U and Th diffusion in natural zircon. Nature 390:159–162

Liu R, Fan Q, Zheng X, Zhang M, Li N (1998) The magma evolution of Tianchi Volcano, Changbaishan. Sci China (Ser D) 41:382–389

Marti J, Gudmundsson A (2000) The Las Cañadas caldera (Tenerife, Canary Islands): an overlapping collapse caldera generated by magma-chamber migration. J Volcanol Geotherm Res 103:161–173. doi:10.1016/S0377-0273(00)00221-3

Masotta M, Gaeta M, Gozzi F, Marra F, Palladino D, Sottili G (2010) $H_2O$-and temperature-zoning in magma chambers: the example of the Tufo Giallo della Via Tiberina eruptions (Sabatini Volcanic District, central Italy). Lithos 118:119–130

Masotta M, Freda C, Gaeta M (2012) Origin of crystal-poor, differentiated magmas: insights from thermal gradient experiments. Contrib Mineral Petrol 163:49–65. doi:10.1007/s00410-011-0658-8

Masotta M, Mollo S, Freda C, Gaeta M, Moore G (2013) Clinopyroxene–liquid thermometers and barometers specific to alkaline differentiated magmas. Contrib Mineral Petrol 166:1545–1561. doi:10.1007/s00410-013-0927-9

Matsubara T, Noro I, Matsuura Y, Irizuki T (2014) Miocene Mollusca from the Ichibu formation on Nishinoshima Island, Oki Islands, Southwest Japan. Paleontol Res 18:6–32. doi:10.2517/2014pr002

McDonough WF, Sun SS (1995) The composition of the Earth. Chem Geol 120:223–253

McGee LE, Smith IEM, Millet M-A, Handley HK, Lindsay JM (2013) Asthenospheric control of melting processes in a monogenetic basaltic system: a case study of the Auckland Volcanic Field, New Zealand. J Petrol 54:2125–2153. doi:10.1093/petrology/egt043

Miyazaki A, Sato K, Saito N (1973) Lead isotopic studies of metamorphic and sedimentary rocks from the Hida metamorphic terrain, Japan. Geochem J 6:105–116

Mollo S, Putirka K, Misiti V, Soligo M, Scarlato P (2013) A new test for equilibrium based on clinopyroxene–melt pairs: clues on the solidification temperatures of etnean alkaline melts at post-eruptive conditions. Chem Geol 352:92–100

Mollo S, Masotta M, Forni F, Bachmann O, De Astis G, Moore G, Scarlato P (2015) A K-feldspar–liquid hygrometer specific to alkaline differentiated magmas. Chem Geol 392:1–8

Morris PA (1986) Geochemistry of some Miocene to Quaternary igneous rocks bordering an ensialic marginal basin—an Example from eastern Shimane Prefecture and Oki Dozen Island, Southwest Japan. Memoirs of the Faculty of Science of Shimane University 20:115–133

Morris PA, Kagami H (1989) Nd and Sr isotope systematics of Miocene to Holocene volcanic rocks from Southwest Japan: volcanism since the opening of the Japan Sea. Earth Planet Sci Lett 92:335–346

Morris PA, Itaya T, Watanabe T, Yamauchi S (1990) Potassium/argon ages of Cenozoic igneous rocks from eastern Shimane Prefecture—Oki Dozen Island, Southwest Japan and the Japan Sea opening. J Southeast Asian Earth Sci 4:125–131. doi:10.1016/0743-9547(90)90011-2

Morris PA, Itaya T, Iizumi S, Kagami H, Watling RJ, Murakami H (1997) Age relations and petrology of alkalic igneous rocks from Oki Dozen, Southwest Japan. Geochem J 31:135–154

Naemura M, Shimada I (1984) Neogene Tertiary of Nishino-shima, Dōzen, Oki Islands. Geological Reports of Shimane University, vol 3, pp 155–160

Nakamura K (1977) Volcanoes as possible indicators of tectonic stress orientation—principle and proposal. J Volcanol Geotherm Res 2:1–16

Nakano S (1998) Calcium distribution patterns in alkali feldspar in quartz syenite from Oki-Dozen, southwest Japan. Mineral Petrol 63:35–48

Nekvasil H (1992) Ternary feldspar crystallization in high-temperature felsic magmas. Am Mineral 77:592–604

Otofuji Y-I, Matsuda T, Nohda S (1985) Paleomagnetic evidence for the Miocene counter-clockwise rotation of Northeast Japan—rifting process of the Japan Arc. Earth Planet Sci Lett 75:265–277

Parsons I, Brown W (1984) Feldspars and the thermal history of igneous rocks. In: Brown W (ed) Feldspars and Feldspathoids, NATO ASI Series, vol 137. Springer, Netherlands, pp 317–371. doi:10.1007/978-94-015-6929-3_9

Parsons I, Lee M (2009) Mutual replacement reactions in alkali feldspars I: microtextures and mechanisms. Contrib Mineral Petrol 157:641–661. doi:10.1007/s00410-008-0355-4

Petrelli M, Poli G, Perugini D, Peccerillo A (2005) PetroGraph: a new software to visualize, model, and present geochemical data in igneous petrology. Geochem Geophy Geosys 6:Q07011. doi:10.1029/2005GC000932

Price RC, Cooper AF, Woodhead JD, Cartwright I (2003) Phonolitic Diatremes within the Dunedin Volcano, South Island, New Zealand. J Petrol 44:2053–2080. doi:10.1093/petrology/egg070

Putirka K, Johnson M, Kinzler R, Longhi J, Walker D (1996) Thermobarometry of mafic igneous rocks based on clinopyroxene-liquid equilibria, 0–30 kbar. Contrib Mineral Petrol 123:92–108. doi:10.1007/s004100050145

Rapp RP, Watson EB, Miller CF (1991) Partial melting of amphibolite/eclogite and the origin of Archean trondhjemites and tonalites. Precambrian Res 51:1–25. doi:10.1016/0301-9268(91)90092-O

Ridolfi F, Renzulli A (2012) Calcic amphiboles in calc-alkaline and alkaline magmas: thermobarometric and chemometric empirical

equations valid up to 1,130 °C and 2.2 GPa. Contrib Mineral Petrol 163:877–895. doi:10.1007/s00410-011-0704-6

Roche O, Druitt TH (2001) Onset of caldera collapse during ignimbrite eruptions. Earth Planet Sci Lett 191:191–202. doi:10.1016/S0012-821X(01)00428-9

Rushmer T (1991) Partial melting of two amphibolites: contrasting experimental results under fluid-absent conditions. Contrib Mineral Petrol 107:41–59

Schmitt AK, Wetzel F, Cooper KM, Zou H, Wörner G (2010) Magmatic longevity of Laacher See Volcano (Eifel, Germany) indicated by U–Th dating of intrusive carbonatites. J Petrol 51:1053–1085. doi:10.1093/petrology/egq011

Schmitz MD, Bowring SA (2001) U–Pb zircon and titanite systematics of the Fish Canyon Tuff: an assessment of high-precision U–Pb geochronology and its application to young volcanic rocks. Geochim Cosmochim Acta 65:2571–2587. doi:10.1016/S0016-7037(01)00616-0

Schwarz S, Klügel A, Wohlgemuth-Ueberwasser C (2004) Melt extraction pathways and stagnation depths beneath the Madeira and Desertas rift zones (NE Atlantic) inferred from barometric studies. Contrib Mineral Petrol 147:228–240. doi:10.1007/s00410-004-0556-4

Seyfried W Jr (1987) Experimental and theoretical constraints on hydrothermal alteration processes at mid-ocean ridges. Ann Rev Earth Planet Sci 15:317–335

Shane P, Martin SB, Smith VC, Beggs KF, Darragh MB, Cole JW, Nairn IA (2007) Multiple rhyolite magmas and basalt injection in the 17.7 ka Rerewhakaaitu eruption episode from Tarawera volcanic complex, New Zealand. J Volcanol Geotherm Res 164:1–26. doi:10.1016/j.jvolgeores.2007.04.003

Sheppard SF, Harris C (1985) Hydrogen and oxygen isotope geochemistry of Ascension Island lavas and granites: variation with crystal fractionation and interaction with sea water. Contrib Mineral Petrol 91:74–81. doi:10.1007/bf00429429

Stormer JCJ, Nicholls J (1978) XLFRAC: a program for the interactive testing of magmatic differentiation models. Comp Geoscie 4:143–159

Sun SS, McDonough WF (1989) Chemical and isotopic systematics of oceanic basalts: implications for mantle composition and processes. In: Saunders AD, Norry MJ (eds) Magmatism in the ocean basins, vol 42. Geological Society Special Publication, Geological Society, London, pp 313–345

Takada A (1994) The influence of regional stress and magmatic input on styles of monogenetic and polygenetic volcanism. J Geophys Res 99:13563–13573

Takahashi E (1978) Petrologic model of the crust and upper mantle of the Japanese island arcs. Bull Volcanol 41:529–547

Tamaki K, Suyehiro K, Allan J, Ingle JC, Pisciotto KA (1992) Tectonic synthesis and implications of Japan Sea ODP drilling. In: Tamaki K, Suyehiro K, Allan J, McWillams M, et al. (eds) Proceedings of the ocean drilling program, science results, vol 127/128 Pt. 2, pp 1333–1348

Tatsumi Y, Shukuno H, Yoshikawa M, Chang Q, Sato K, Lee MW (2005) The petrology and geochemistry of volcanic rocks on Jeju Island: plume magmatism along the Asian continental margin. J Petrol 46:523–553. doi:10.1093/petrology/egh087

Tatsumoto M, Nakamura Y (1991) DUPAL anomaly in the Sea of Japan: Pb, Nd, and Sr isotopic variations at the eastern Eurasian continental margin. Geochim Cosmochim Acta 55:3697–3708

Tiba T (1986) Alkalic Volcanism at Oki-Dōzen. Memoirs of the National Science Museum, Tokyo 19:19–27

Tiba T, Kaneko N, Kano K (2000) Geology of the Uragō District—with 1:50,000 geological sheet map. (in Japanese with English abstract)

Toshida K, Miura D, Hataya R (2006) Proposition of assessment method for lateral magma migration—effects of magma geochemistry studied from the distribution of conduits at Oki Dozen volcano. CRIEPI, Abiko

Valentine GA, Krogh KEC (2006) Emplacement of shallow dikes and sills beneath a small basaltic volcanic center—the role of preexisting structure (Paiute Ridge, southern Nevada, USA). Earth Planet Sci Lett 246:217–230

Villemant B (1988) Trace element evolution in the Phlegrean Fields (Central Italy): fractional crystallization and selective enrichment. Contrib Mineral Petrol 98:169–183. doi:10.1007/bf00402110

Wada Y, Itaya T, Ui T (1990) K–Ar ages of Oki-Dozen and Tango dike Swarms, Western Honshu, Japan. Bull Volcanol Soc Japan 35:217–229

Wark DA, Hildreth W, Spear FS, Cherniak DJ, Watson EB (2007) Pre-eruption recharge of the Bishop magma system. Geology 35:235–238. doi:10.1130/g23316a.1

Watson EB, Harrison TM (1983) Zircon saturation revisited: temperature and composition effects in a variety of crustal magma types. Earth Planet Sci Lett 64:295–304

Weaver BL (1991) The origin of ocean island basalt end-member compositions: trace element and isotopic constraints. Earth Planet Sci Lett 104:381–397

Wei H, Wang Y, Jin J, Gao L, Yun SH, Jin B (2007) Timescale and evolution of the intracontinental Tianchi volcanic shield and ignimbrite-forming eruption, Changbaishan, Northeast China. Lithos 96:315–324

White JC, Parker DF, Ren M (2009) The origin of trachyte and pantellerite from Pantelleria, Italy: insights from major element, trace element, and thermodynamic modelling. J Volcanol Geotherm Res 179:33–55. doi:10.1016/j.jvolgeores.2008.10.007

Wörner G, Schmincke H-U (1984) Petrogenesis of the zoned Laacher See Tephra. J Petrol 25:836–851. doi:10.1093/petrology/25.4.836

Xu J et al (2012) Recent unrest of Changbaishan volcano, northeast China: a precursor of a future eruption? Geophys Res Lett 39:L16305. doi:10.1029/2012gl052600

Zimanowski B, Büttner R, Lorenz V, Häfele H-G (1997) Fragmentation of basaltic melt in the course of explosive volcanism. J Geophys Res 102:803–814. doi:10.1029/96jb02935

Zindler A, Hart S (1986) Chemical geodynamics. Ann Rev Earth Planet Sci 14:493–571